FEDERAL UNIVERSITY OF SÃO CARLOS
CENTER FOR SCIENCE AND TECHNOLOGY
GRADUATE PROGRAM IN PHYSICS

QUANTUM MEMORY BASED ON ELECTROMAGNETICALLY INDUCED TRANSPARENCY IN OPTICAL CAVITIES

ROMMEL RODRIGUES DE OLIVEIRA

São Carlos
April/2015

FEDERAL UNIVERSITY OF SÃO CARLOS
CENTER FOR SCIENCE AND TECHNOLOGY
GRADUATE PROGRAM IN PHYSICS

QUANTUM MEMORY BASED ON ELECTROMAGNETICALLY INDUCED TRANSPARENCY IN OPTICAL CAVITIES

ROMMEL RODRIGUES DE OLIVEIRA

Dissertation submitted to the Graduate Program in Physics of the Federal University of São Carlos as part of the requirements for obtaining the title of Master in Physics.

Supervisor: Prof. Dr. Celso Jorge Villas-Bôas

São Carlos
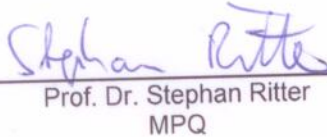April/2015

UNIVERSIDADE FEDERAL DE SÃO CARLOS

Centro de Ciências Exatas e de Tecnologia
Programa de Pós-Graduação em Física

Folha de Aprovação

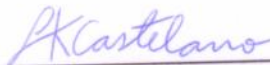Assinaturas dos membros da comissão examinadora que avaliou e aprovou a Defesa de Dissertação de Mestrado do candidato Rommel Rodrigues de Oliveira, realizada em 16/04/2015:

Prof. Dr. Celso Jorge Villas Boas
UFSCar

Prof. Dr. Stephan Ritter
MPQ

Prof. Dr. Leonardo Kleber Castelano
UFSCar

Dedication

To my parents, Luiz Carlos de Oliveira and Soraia Rodrigues de Oliveira, without whom I wouldn't be where I am today.

"If you're gonna do something, do it right. You don't always have to be the number one, but always give your best to be one of the greatest."
Luiz Carlos de Oliveira

Acknowledgments

First of all, I would like to thank my parents, Luiz Carlos de Oliveira and Soraia Rodrigues de Oliveira. For all the support they gave me through the years, for inspiring me to always aim high and dream big, for teaching me the value of hard work and education, and for all the sacrifices they made for me and my brothers so we could have a better life than theirs. They are true heroes, my best friends, and the best parents anyone could wish for and that I love with all my heart. A heartfelt thanks also goes to both my grandmothers, Maria Marlene Lourenço and Marlene Candida de Oliveira whose I couldn't be more grateful to have present in my life. And a specially sincere thanks to my late maternal grandfather, Jacob Rodrigues, my late paternal great-grandparents, Luzia Candida de Jesus and Henrique Gonçales, and my late maternal great-grandfather, Francisco Lourenço Dias, who've always believed in me and I wished were here for this moment.

I would also like to thank Renato Molina Toth, a friend for several years now, and César Rodrigues de Oliveira, my brother and friend since he was born, for sharing both aspirations and frustrations, and several glasses of beer, making this journey way easier with the company of those two. A special thanks also goes to Aparecido Marandola Jr., a personal friend and friend of the family who is always there, for good and bad times. And I shouldn't forget to mention my youngest brother, Maurício Rodrigues de Oliveira, who is still young and I'm sure still has wonderful things reserved in his future.

A very special thanks goes to my supervisor, Prof. Dr. Celso Jorge Villas-Bôas. I've been working with him for several years now, and I have nothing but to thank him for. Everything I know about research in physics I've learned with him, who took the time and patience to teach me everything he could. All my accomplishments in this field are due to the special care he took with me when I was just a young undergrad student aspiring for a career in physics.

I would also like to thank my friend and work colleague Prof. Dr. James Alves de Souza for all conversations, both physics and non-physics related, and for making the work environment at the university a better place to be. A special thanks also goes to Mariana Victória Ballottin, a very special friend inside and outside the physics department, whose company kept me sane during the hard times and kept me joyful during the happy ones.

I would also like to thank Prof. Rempe's group, for hosting me and Prof. Celso for a week in their facilities during the final stage of this thesis, whose fruitful discussions provided amazing insights on our final results.

Finally, I would also like to thank the Brazilian National Council for Science and Technology Development (CNPq) for the scholarship I was granted during my master; The Graduate Program in Physics (PPGF) of the Center for Science and Technology (CCET) of the Federal University of São Carlos (UFSCar) and the Brazilian National Institute for Science and

Abstract

Recently a quantum memory for a coherent pulse was accomplished using an atom trapped inside a high finesse cavity, where an efficiency of 9.3% was achieved for a storage time of $2\mu s$ and an average fidelity of 93% for a storage time of $180\mu s$. We theoretically studied this system using the master equation approach, exhausting all the possible ways one could improve the efficiency, defined here as the ratio between the mean number of photons retrieved after the memory process and the mean number of photons that enters the empty cavity, $\eta = \langle a^\dagger a \rangle_{out} / \langle a^\dagger a \rangle_{in}$, which proved to have an upper bound of 25%. Since protocols relying on phase-matching conditions for single photon input states were already developed, using a model by H. Carmichael, a comparison between storage of coherent and single photon states was made, which did not gave rise any observable difference. Finally a more detailed study about the differences between an input-output and a master equation approach was done. It was concluded that the experimental setup suitable for observing cavity electromagnetically induced transparency (EIT) is not the ideal one for a quantum memory experiment. No modifications to the master equation theory were necessary, and a simple relation between the cavity and output fields was derived.

Resumo

Recentemente uma memória quântica para um pulso coerente foi realizada utilizando um átomo aprisionado em uma cavidade de alta finesse, onde uma eficiência de 9.3% foi alcançada para um tempo de armazenamento de $2\mu s$ e uma fidelidade média de 93% para um tempo de armazenamento de $180\mu s$. Esse sistema foi estudado teoricamente utilizando a abordagem da equação mestra, exaustando todos os possíveis métodos para melhorar a eficiência, definida aqui como a razão entre o número médio de fótons recuperados depois do processo da memória e o número médio de fótons que entra na cavidade vazia, $\eta = \langle a^{\dagger}a \rangle_{out}/\langle a^{\dagger}a \rangle_{in}$, que mostrou ter um limite superior de 25%. Uma vez que protocolos baseados em condições de casamento de fase para estados de entrada de um fóton já haviam sido desenvolvidos, utilizando um modelo feito por H. Carmichael, uma comparação entre o armazenamento de estados coerente e de um fóton foi feita, a qual não levantou nenhuma diferença observável. Finalmente um estudo mais detalhado sobre as diferenças entre uma teoria de input-output e equação mestra foi feito. Concluiu-se que o arranjo experimental utilizado para observar transparência eletromagneticamente induzida (*electromagnetically induced transparency - EIT*) em cavidades não é adequado para um experimento de memória quântica. Nenhuma modificação à teoria de equação mestra foi necessária, e uma simples relação entre os campos na cavidade e fora dela foi derivada.

Table of Contents

Chapter 1

Introduction

With the growing improvement of computer's processing power, Gordon Moore, Intel's co-founder, made a prediction: the computing power will double, maintaining a constant price, approximately every two years. This means that every couple of years the number of transistors in a processor will double, which implies in reducing the size of a transistor so that it is possible to fit twice as many of them in the same space as before. This prediction became known as Moore's Law.

Transistors are inherently quantum, i.e., their behavior can only be explained with the laws of quantum mechanics, although in a classical circuit they only work as a valve. Nevertheless, Moore's Law establishes a limit for how small a transistor can be. Thus, it is necessary to seek another way to increase computing power, that is not by increasing the number of transistors. At this point enters quantum computation.

In the 1980s, the research field of quantum computation starts to take shape. Analogously to the Turing machine, in 1985 David Deutsch proposes an universal quantum computer, a model in which the operations and the algorithms' logic are based on the principles of quantum mechanics [1].

In classical computation the information is coded in a binary system. The smallest unit of information is the *bit*, and it can take two values: 0 or 1. Hence, in a system with n bits, *n pieces of information* are required to determine a certain state: if each one of the n bits is either on (1) or off (0). In quantum computation, in addition to the states that are encountered in classical computation, the *quantum bits*, or *qubits*, can assume any superposition between the classical states, so that for a system with n qubits, 2^n *pieces of information* are required to completely describe a state [1]. For $n = 500$, 2^{500} is greater than the estimated number of atoms in the universe. The goal of quantum computation is to use this amount of information that quantum systems are able to manipulate, to create faster and more efficient algorithms than their classical analogues, or even perform tasks that before were impossible, such as simulate more complex quantum systems [2].

An essential element for quantum computation is a quantum memory [3]. This device can be defined as a system capable of storing quantum states to perform a certain task. Quantum memories can be applied not only in quantum computation but also in quantum repeaters, metrology, detection and emission of single photons, and as a system to study fundamental aspects of quantum mechanics [4]. Among the physical systems used to its implementation are solid state atomic ensembles, nitrogen vacancy centers, quantum dots, systems with a single atom, quantum gases and optical phonons in diamond [5].

Here a system composed of a single atom trapped in an optical cavity stores an input state in the atom's electronic levels by means of the electromagnetically induced transparency (EIT). Recently a quantum memory was accomplished using this system, where an efficiency of 9.3% was achieved for a storage time of $2\mu s$ and an average fidelity of 93% for a storage time of $180\mu s$ [6]. It is interesting to optimize the storage efficiency of this system for applications such as quantum repeaters, which may require the efficiency to be greater than 90% [4], and linear optical quantum computation, which may require an efficiency above 99% [4].

Two approaches were used in this work. First a master equation formalism [7], a traditional method to include dissipation in open quantum systems. Later, an input-output theory [8] was explored as a way to investigate details that might have been overlooked in the master equation approach.

Chapter 2

Electromagnetically induced transparency

In this chapter we will briefly present the theoretical background needed for understanding cavity EIT. We begin with the Jaynes-Cummings model, that describes a coherent energy exchange between atom and field. Afterwards we present the basics aspects of EIT in free space. Finally, EIT in optical cavities is introduced and briefly discussed.

2.1 Jaynes-Cummings model

The Jaynes-Cummings Hamiltonian, that describes a coherent energy exchange between atom and field is, in the Schrödinger picture, given by [9]

$$H_{JC} = \hbar\omega_0\sigma_{ee} + \hbar\omega a^\dagger a + \hbar g(a\sigma_{eg} + a^\dagger\sigma_{ge}). \tag{2.1}$$

In this Hamiltonian ω_0 and ω are respectively the atomic transition and the cavity mode frequencies; g is the atom-field coupling (vacuum's Rabi frequency); a ($a^\dagger$) is the annihilation (creation) operator of the field; and $\sigma_{ij} = |i\rangle\langle j|$, $i, j = e, g$, where $|g\rangle$ is the atom's ground state and $|e\rangle$ is its excited state.

It is important to remember that two approximations were made to reach this model: the dipole approximation, valid when the wave length of the impinging radiation is large in comparison with the atomic radius, and the rotating wave approximation, that discards rapid oscillating terms that have a negligible contribution to the system's dynamics, valid in the limit when the atom-field coupling is small in comparison to the characteristics frequencies of the system.
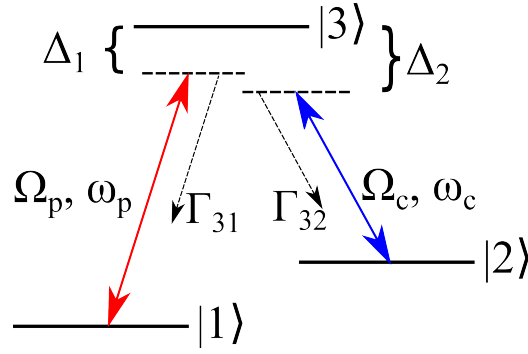
Figure 2.1: Diagram of levels involved in an usual EIT process.

2.2   EIT in free space

In this section we analyze the problem of an atomic sample that consists of 3 level atoms interacting with two classical fields. Levels $|1\rangle$ and $|2\rangle$ are the ground states, and there is no dipole transition between them. Level $|3\rangle$ is the excited state, and it can decay both to level $|2\rangle$ as well as to $|1\rangle$. Interacting with the transition $|1\rangle \leftrightarrow |3\rangle$ is a probe field with Rabi frequency Ω_P and frequency ω_P, and interacting with the transition $|2\rangle \leftrightarrow |3\rangle$ there is a control field with Rabi frequency Ω_C and frequency ω_C. There is a detuning Δ_1 between the frequencies of the probe field and the transition $|1\rangle \leftrightarrow |3\rangle$, ω_{31}, and a detuning Δ_2 between the frequencies of the control field and the transition $|2\rangle \leftrightarrow |3\rangle$, ω_{32}. The polarization decay rate related to the $|1\rangle \leftrightarrow |3\rangle$ transition is Γ_{31} and the polarization decay rate related to the $|2\rangle \leftrightarrow |3\rangle$ is Γ_{32}. Such setup is called Λ configuration and is illustrated in Figure 2.1.

Adopting $|1\rangle$ as our zero energy, the system's Hamiltonian $H = H_0 + H_{int}$ is given by

$$H = \omega_3 \sigma_{33} + \omega_2 \sigma_{22} + \{\Omega_P(t)\sigma_{31}e^{-i\omega_P t} + \Omega_C(t)\sigma_{32}e^{-i\omega_C t} + h.c.\}, \tag{2.2}$$

where

$$H_0 = \omega_3 \sigma_{33} + \omega_2 \sigma_{22},$$

and

$$H_{int} = \{\Omega_P(t)\sigma_{31}e^{-i\omega_P t} + \Omega_C(t)\sigma_{32}e^{-i\omega_C t} + h.c.\}.$$

Here $h.c.$ stands for hermitian conjugate, and $\sigma_{ij} = |i\rangle\langle j|$ $(i,j = 1,2,3)$ are the atomic operators that describe the level populations $(i = j)$, and the transitions between them $(i \neq j)$. It is worth reminding that from this point on we use $\hbar = 1$ to simplify the notation.

Going to the interaction picture, through a unitary transformation $U = e^{-iH_0 t}$, we have that the interaction Hamiltonian $\tilde{H}_I$, that describes the dynamics of two classical fields acting on a atomic sample, is given by

$$\tilde{H}_I = \{\Omega_P(t)\sigma_{31}e^{i\Delta_1 t} + \Omega_C(t)\sigma_{32}e^{i\Delta_2 t} + h.c.\}, \tag{2.3}$$

with $\Delta_1 = \omega_{31} - \omega_p$ ($\omega_{31} = \omega_3$) and $\Delta_2 = \omega_{32} - \omega_c$ ($\omega_{32} = \omega_3 - \omega_2$). Removing the time dependency, through a unitary transformation, $U = e^{i(\Delta_1\sigma_{33} - (\Delta_2 - \Delta_1)\sigma_{22})t}$, the new Hamiltonian is given by

$$H_I = \Delta_1\sigma_{33} + (\Delta_1 - \Delta_2)\sigma_{22} + (\Omega_P\sigma_{31} + \Omega_C\sigma_{32} + h.c.). \tag{2.4}$$

Equation 2.4 has three eigenenergies and eigenstates. One of them is a dark state with a zero eigenenergy, $\lambda_0 = 0$, which is given by

$$|D\rangle = cos\theta|1\rangle - sin\theta|2\rangle, \tag{2.5}$$

where

$$tan(\theta) = \frac{\Omega_P}{\Omega_C}.$$

To visualize the effects of the field on the atomic medium one must calculate the electric susceptibility of the medium. The polarization of a material medium is given by

$$\vec{P} = \chi_e\vec{E},$$

where χ_e is the medium's linear susceptibility, with

$$Re(\chi_e) \rightarrow \text{medium's dispersion,}$$

$$Im(\chi_e) \rightarrow \text{medium's absorption.}$$

The polarization can also be written as

$$\vec{P} = \sum_i \frac{\langle\vec{\mu}_i\rangle}{V} = \frac{N}{V}Tr(\rho\vec{\mu}),$$

where N is the total number of atoms in the volume V and ρ is the density matrix of the system. Here we are working on the limit of low atomic densities, with non-interacting atoms. For a 3 level atom the most general density operator (in Schrödinger picture) can be written as

$$\rho = \rho_{11}|1\rangle\langle1| + \rho_{22}|2\rangle\langle2| + \rho_{33}|3\rangle\langle3| + (\rho_{21}e^{-i\omega_{21}t}|2\rangle\langle1| + \rho_{31}e^{-i\omega_{31}t}|3\rangle\langle1| + \rho_{32}e^{-i\omega_{32}t}|3\rangle\langle2| + h.c.),$$

and the dipole moment operator is given by

$$\vec{\mu} = \vec{\mu}_{13}|1\rangle\langle3| + \vec{\mu}_{23}|2\rangle\langle3| + h.c. \ .$$

Thus

$$\vec{P} = \frac{N}{V}(\vec{\mu}_{13}\rho_{31}e^{-i\omega_{31}t} + \vec{\mu}_{23}\rho_{32}e^{-i\omega_{32}t} + h.c.).$$

The terms ρ_{31} and ρ_{32} and their complex conjugates may be obtained through the master equation for this system [7]

$$\frac{d\rho}{dt} = -i[H_I, \rho] + \Gamma_{31}(2\sigma_{13}\rho\sigma_{31} - \sigma_{33}\rho - \rho\sigma_{33}) + \Gamma_{32}(2\sigma_{23}\rho\sigma_{32} - \sigma_{33}\rho - \rho\sigma_{33})$$
$$+ \gamma_2(2\sigma_{22}\rho\sigma_{22} - \sigma_{22}\rho - \rho\sigma_{22}) + \gamma_3(2\sigma_{33}\rho\sigma_{33} - \sigma_{33}\rho - \rho\sigma_{33}),$$

(2.6)

where γ_2 and γ_3 are the dephasing rates of the levels 2 and 3.

Here H_I is given by Equation 2.4. However it is important to remember that with the Hamiltonian H_I we are at the rotating frame and, once the solution is obtained, one must go back to the Schrödinger picture.

Knowing that

$$\langle i|\rho|j\rangle \equiv \rho_{ij} \qquad and \qquad \langle i|\dot{\rho}|j\rangle \equiv \dot{\rho}_{ij},$$

taking the asymptotic limit, i.e., $\dot{\rho}_{ij} = 0$, and the limit in which $|\Omega_P| \ll |\Omega_C|$, that implies $\rho_{11} \simeq 1$, $\rho_{22} \simeq 0$ and $\rho_{33} \simeq 0$, it is possible to obtain the elements of ρ. In the interaction picture [10]

$$\rho_{31} = \frac{2i\Omega_P[2\gamma_{21} + 2i(\Delta_1 - \Delta_2)]}{(2\gamma_{31} + 2i\Delta_1)[2\gamma_{21} + 2i(\Delta_1 - \Delta_2)] + 4\Omega_C^2}e^{i\Delta_1 t}$$

and

$$\rho_{32} = \frac{-i8\Omega_P^2\Omega_C e^{i\Delta_2 t}}{(2\gamma_{32} + 2i\Delta_2)\{(2\gamma_{31} - 2i\Delta_1)[2\gamma_{21} - 2i(\Delta_1 - \Delta_2)] + 4\Omega_C^2\}},$$

where $\gamma_{31} = \Gamma_{31} + \Gamma_{32} + \gamma_3$, $\gamma_{32} = \Gamma_{31} + \Gamma_{32} + \gamma_3 + \gamma_2$ and $\gamma_{12} = \gamma_2$. Recalling that $\Delta_1 = \omega_{31} - \omega_P$ e $\Delta_2 = \omega_{32} - \omega_C$, and defining $\Delta \equiv \Delta_1$ and $\delta \equiv \Delta_1 - \Delta_2$

$$\vec{P} = \frac{N}{V}\{\vec{\mu}_{13}\frac{2i\Omega_P[2\gamma_{21} + 2i\delta]}{(2\gamma_{31} + 2i\Delta)[2\gamma_{21} + 2i\delta] + 4\Omega_C^2}e^{-i\omega_P t} + c.c$$

$$-\vec{\mu}_{23}\frac{-8i\Omega_P^2\Omega_C e^{-i\omega_C t}}{(2\gamma_{32} + 2i(\Delta - \delta))\{(2\gamma_{31} - 2i\Delta)[2\gamma_{21} - 2i\delta] + 4\Omega_C^2\}} + c.c\},$$

with c.c. meaning the complex conjugate. On the other hand, $\vec{P} = \chi_e\vec{E}$ and $\vec{E} = \vec{E}_P e^{-i\omega_P t} + \vec{E}_C e^{-i\omega_C t} + c.c.$ Since we are interested in the medium's response to the probe field, we take the term with $e^{-i\omega_P t}$ and its complex conjugate. Therefore

$$\chi^{(1)}(-\omega_P, \omega_P) = \frac{N}{V}|\vec{\mu}_{13}|2\Omega_P\frac{i[2\gamma_{21} + 2i\delta]}{(2\gamma_{31} + 2i\Delta)[2\gamma_{21} + 2i\delta] + 4\Omega_C^2},$$

(2.7)

whose real part is given by

$$Re(\chi^{(1)}) = \frac{N}{V}|\vec{\mu}_{13}|2\Omega_P\frac{2\gamma_{21}[4\gamma_{31}(\Delta - \delta) + 4\gamma_{21}\Delta] + \delta[8\Delta\delta - 8\Omega_C^2]}{|(2\gamma_{31} + 2i\Delta)[2\gamma_{21} + 2i\delta] + 4\Omega_C^2|^2},$$
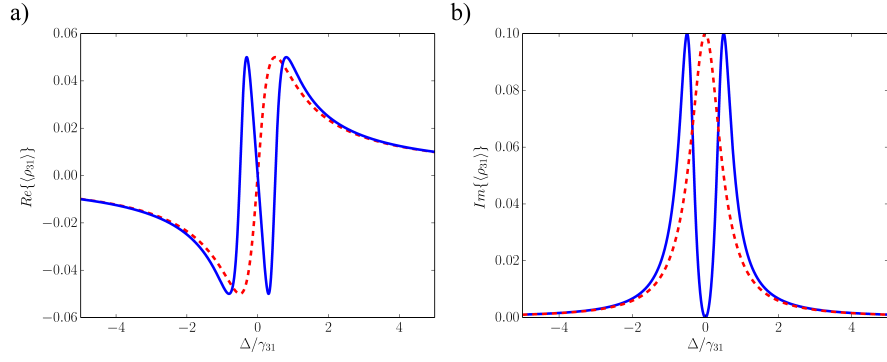
(2.8)

Figure 2.2: Electromagnetically induced transparency characteristic curves. In the blue solid curve the control field is on, while in the red dashed curve the control field is off. a) Real part of ρ_{31}, which is proportional to the atomic medium's dispersion. b) Imaginary part of ρ_{31}, that is proportional to the medium's absorption. The values used here were: $\gamma_{31} = 1MHz$, $\gamma_{21} = 0$, $\delta = 0$, $\Omega_p = 0.1\gamma_{31}$, and $\Omega_c = \gamma_{31}$ in the blue solid curve and $\Omega_c = 0$ in the red dashed curve.

and its imaginary part by

$$Im(\chi^1) = \frac{N}{V}|\vec{\mu}_{13}|2\Omega_P \frac{2\gamma_{31}(4\gamma_{21}^2 + 4\delta^2) + 8\gamma_{21}\Omega_C^2}{|(2\gamma_{31} + 2i\Delta)[2\gamma_{21} + 2i\delta] + 4\Omega_C^2|^2}. \tag{2.9}$$

Figure 2.2 shows the real and imaginary parts of ρ_{31}, for $\Omega_c = 0$ and $\Omega_c \neq 0$. The Equations 2.8 and 2.9 are proportional to the real and imaginary parts of ρ_{31}, respectively.

We can see in Figure 2.2 a) the real part of ρ_{31}, which is proportional to the medium's dispersion. When the control field is turned on, solid blue curve, one can see a rapid variation in the medium's dispersion for a small change in the detuning. This will lead to the phenomenon of slow light, since the light's velocity in a medium is inversely proportional to the derivative of the medium's dispersion. Figure 2.2 b) shows the imaginary part of ρ_{31}, which is proportional to the medium's absorption. In the solid blue curve, which depicts the situation when the control field is on, one can see the effect of turning the control field on: it creates a minimum in the absorption when the detuning is null, i.e., the medium is now transparent to the probe field when the control field is on. This is the basic principle of EIT, making a medium transparent to a certain wavelength by shining it with light of a different wavelength.

2.3 EIT in optical cavities

In this section a system consisting of a 3 level atom in the Λ configuration inside a high finesse cavity will be analyzed. The cavity mode, of frequency ω, interacts with the transition $|1\rangle \leftrightarrow |3\rangle$ with a coupling rate g (Rabi frequency). Interacting with transition $|2\rangle \leftrightarrow |3\rangle$ there is a control field with Rabi frequency Ω_C and frequency ω_C. There is also a pumping in the cavity (probe field) given by $\varepsilon(\omega_p, t) = \varepsilon a e^{i\omega_p t} + \varepsilon^* a^\dagger e^{-i\omega_p t}$. The experimental setup is assembled in such
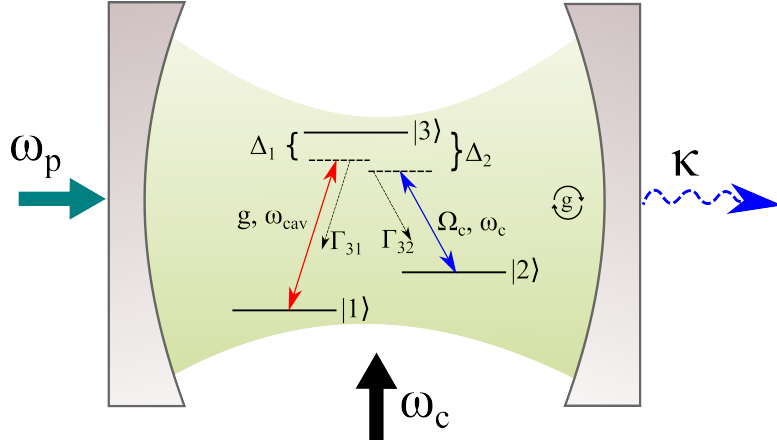
Figure 2.3: Electromagnetically induced transparency inside an optical cavity.

a way that an intense probe field impinges on the left cavity mirror, which has a very high reflectivity. Only a small portion of light is transmitted, and we calculate the interaction of it with the atom inside the cavity. The right mirror has a smaller reflectivity than the left one, so that light leaves the cavity preferably through the right side of it, where a detector is placed to make transmission measurements. This system is illustrated in Figure 2.3.

Setting $|1\rangle$ as zero energy, the system's Hamiltonian is given by

$$H = \omega_3\sigma_{33} + \omega_2\sigma_{22} + \omega a^\dagger a + (ga\sigma_{31} + \Omega_C\sigma_{32}e^{-i\omega_C t} + \varepsilon ae^{i\omega_p t} + h.c.), \qquad (2.10)$$

where

$$H_0 = \omega_3\sigma_{33} + \omega_2\sigma_{22} + \omega a^\dagger a,$$

$$H_{int} = (ga\sigma_{31} + \Omega_C\sigma_{32}e^{-i\omega_C t} + \varepsilon ae^{i\omega_p t} + h.c.).$$

In the interaction picture, obtained through the unitary transformation $U_0 = e^{-iH_0 t}$, we have

$$H_I = (ga\sigma_{31}e^{i\Delta_1 t} + \Omega_C\sigma_{32}e^{i\Delta_2 t} + \varepsilon ae^{i\Delta t} + h.c.) , \qquad (2.11)$$

where

$$\Delta_1 = \omega_3 - \omega \text{: detuning between atom and cavity,}$$

$$\Delta_2 = (\omega_3 - \omega_2) - \omega_C \text{: detuning between atom and control field,}$$

$$\Delta = \omega_p - \omega \text{: detuning between probe field and cavity.}$$

Taking the time dependency through $U_1 = e^{-i[\Delta a^\dagger a - \Delta_1\sigma_{33} - (\Delta_1 - \Delta_2)\sigma_{22} - \Delta\sigma_{11}]t}$, we get the Hamiltonian [11]

$$H_I = \Delta_1\sigma_{33} + (\Delta_1 - \Delta_2)\sigma_{22} + \Delta\sigma_{11} - \Delta a^\dagger a + (\varepsilon a + ga\sigma_{31} + \Omega_C\sigma_{32} + h.c.). \qquad (2.12)$$
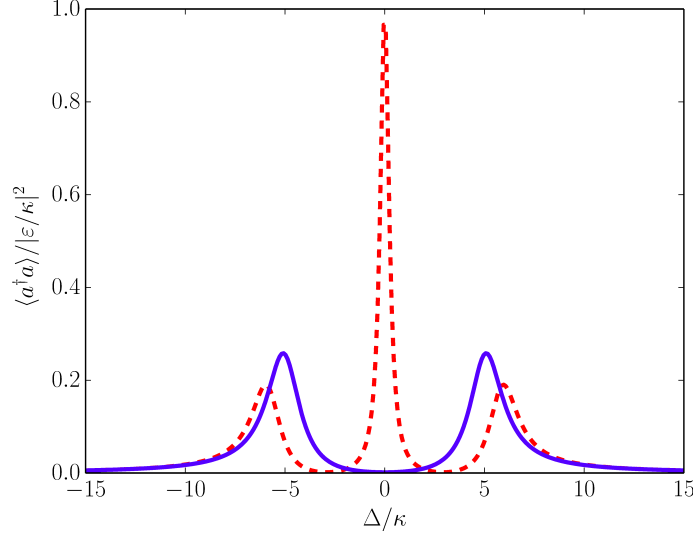
Figure 2.4: Normalized transmission ($\langle a^{\dagger}a\rangle/|\varepsilon/\kappa|^2$) as a function of the detuning between cavity and probe field. The parameters used here were $\kappa = 1MHz$, $g = 5\kappa$, $\Omega_C = 3\kappa$ in the red dashed curve and $\Omega_C = 0$ in the blue solid curve, $\Gamma_{31} = 1\kappa$, $\Gamma_{32} = 0$, $\gamma_2 = 0$, $\gamma_3 = 0$, $\Delta_1 = \Delta_2 = 0$, $\varepsilon = \sqrt{0.01}\kappa$.

The master equation for this system is given by

$$\frac{d\rho}{dt} = -i[H_I, \rho] + \kappa(2a\rho a^{\dagger} - a^{\dagger}a\rho - \rho a^{\dagger}a)$$
$$+\Gamma_{31}(2\sigma_{13}\rho\sigma_{31} - \sigma_{33}\rho - \rho\sigma_{33}) + \Gamma_{32}(2\sigma_{23}\rho\sigma_{32} - \sigma_{33}\rho - \rho\sigma_{33})$$
$$+\gamma_2(2\sigma_{22}\rho\sigma_{22} - \sigma_{22}\rho - \rho\sigma_{22}) + \gamma_3(2\sigma_{33}\rho\sigma_{33} - \sigma_{33}\rho - \rho\sigma_{33})$$

(2.13)

where κ is the cavity field decay rate, Γ_{32} and Γ_{31} are the polarization decay rates related to the $|2\rangle \leftrightarrow |3\rangle$ and to the $|1\rangle \leftrightarrow |3\rangle$ transitions, respectively, and γ_2 and γ_3 are the dephasing rates of the levels 2 and 3, respectively. Figure 2.4 shows the normalized transmission from the cavity, obtained through the master equation, when the control field is off and on, clearly showing the transparency window provided by the EIT. It is important to remember that the condition $\Gamma_{32} = 0$ used in this graph is a bit artificial. In reality Γ_{32} never is exactly null for a three level atom, and graphs of this kind, for when the control field is off (red dashed curve), are only obtained by making measurements in a time when the system did not reach the full stationary state, and the atom can be considered as a two level system, i.e., $\Gamma_{32} \simeq 0$.

The main advantage of using cavity EIT instead of EIT in free space, is the significant rise in the atom-field coupling provided by the cavity. With a higher coupling, the transference of the field states to the atom happen in a more coherent way, being less susceptible to dissipative effects and decoherence.

Chapter 3

Quantum memory

In this chapter we are going to explain the basic principles of a quantum memory and see the methods we are going to use to study it. It should be clear to the reader that, although here we are using a simpler version of the quantum memory, where the qubits are 0 and 1 photons, in the experiment [6] the qubits were implemented using polarization states, σ_+ and σ_-. Our simplification should not affect the results, since the system used for the polarization states can be seen as two three level systems, as it can be seen in Figure 3.1. It should also be clear the difference we are making between single sided and two sided cavities. In a single sided cavity, we probe it through the less reflective mirror and measure the outcome through the same side. In a two sided cavity, we probe the cavity through the more reflective mirror and measure the outcome through the less reflective one. Cavity EIT is done with a two sided cavity, and since we are studying a memory based on cavity EIT, our model will also consist of a two sided cavity.
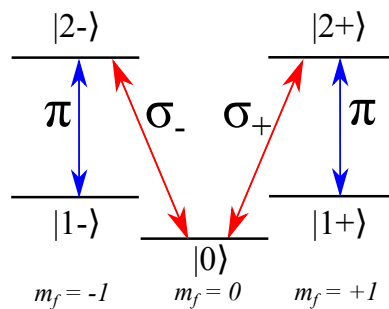

Figure 3.1: 5 level atom diagram. Here we have three ground states, $|-1\rangle$, $|0\rangle$ and $|+1\rangle$, and two excited states, $|-2\rangle$ and $|+2\rangle$. The control field, with linear polarized light, couples the transitions $|-1\rangle \leftrightarrow |-2\rangle$ and $|+1\rangle \leftrightarrow |+2\rangle$. The cavity, with circularly polarized light couples the transitions $|0\rangle \leftrightarrow |+2\rangle$ and $|0\rangle \leftrightarrow |-2\rangle$. This structure is symmetric, and can be seen as two three level atoms.

3.1 Basic principles

The main objective of this work was to study the storage and recovery process in an optical quantum memory based on cavity EIT, as accomplished in [6], so that the efficiency of the device be optimized, within the available experimental conditions. The efficiency is defined as the ratio between the mean number of photons retrieved after the memory process and the mean number of photons that enters the empty cavity, i.e., $\eta = \langle a^\dagger a \rangle_{out} / \langle a^\dagger a \rangle_{in}$.

The principle behind EIT based quantum memories is to use the transparency window generated by the phenomenon. For an ensemble of atoms, first one must prepare them in the ground state $|1\rangle$ which, in the limit where $\Omega_c \gg \Omega_p$, is a dark-state of the system. If instead of a probe field, a pulse with one photon is sent, with frequency spectrum within the transparency window, with the control field on this pulse is not absorbed. However, if one adiabatically turns off the control field, keeping the system in the dark-state, the pulse is now absorbed and the dark-state is now $|2\rangle$.

Similarly, if the efficiency of the process is high enough, one can send a pulse with a superposition of 0 and 1 photon. Adiabatically turning off the control field will store this superposition in the atomic levels.

For a single atom in a cavity, when the field has at most one excitation, the dark-state is, according to Equation 2.12, given by [12]

$$|D\rangle = -i\frac{\Omega_c |1\rangle_{\text{atom}}|1\rangle_{field} - g|2\rangle_{\text{atom}}|0\rangle_{field}}{\sqrt{\Omega_c^2 + g^2}}.$$

If $\Omega_c \gg g \Rightarrow |D\rangle \simeq |1\rangle_{\text{atom}}|1\rangle_{field}$. If $\Omega_c \ll g \Rightarrow |D\rangle \simeq |2\rangle_{\text{atom}}|0\rangle_{field}$. Therefore, if the initial state is $|\psi(0)\rangle = |1\rangle_{\text{atom}}|1\rangle_{field}$, and $\Omega_c \gg g$, turning off the control field adiabatically, according to the adiabatic theorem [13], the system will remain in the dark state which eventually will be $|\psi(t_{final})\rangle = |2\rangle_{\text{atom}}|0\rangle_{field}$

Below we have an example of how this would work. Consider an initial state for the light given by

$$|\psi\rangle = \alpha|0\rangle_{field} + \beta|1\rangle_{field}.$$

So now we have

$$(\alpha|0\rangle_{field} + \beta|1\rangle_{field})|1\rangle_{\text{atom}} = \alpha|0\rangle_{field}|1\rangle_{\text{atom}} + \beta|1\rangle_{field}|1\rangle_{\text{atom}}.$$

Adiabatically turning off the control field, the atom can absorb one excitation of the field, thus

$$\alpha|0\rangle_{field}|1\rangle_{\text{atom}} + \beta|1\rangle_{field}|1\rangle_{\text{atom}} \xrightarrow[\text{ideal}]{(\Omega_c \to 0)} \alpha|0\rangle_{field}|1\rangle_{\text{atom}} + \beta|0\rangle_{field}|2\rangle_{\text{atom}}.$$
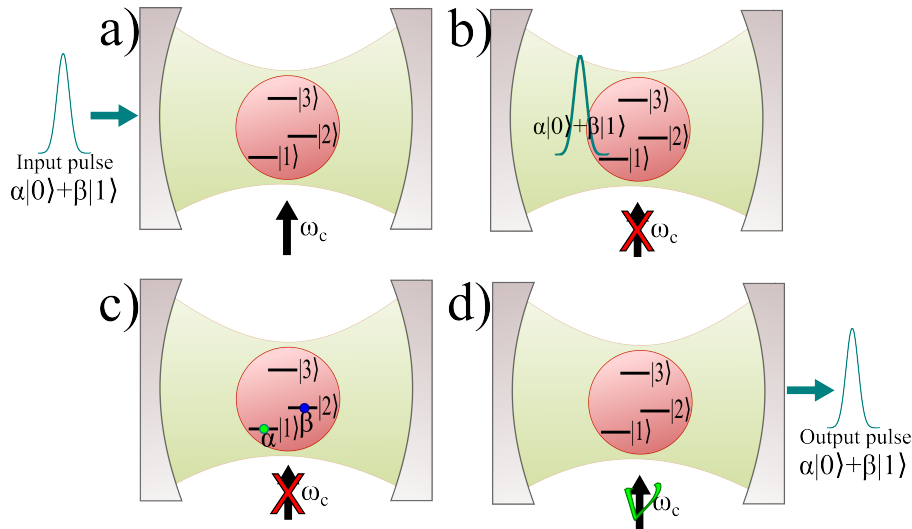
Figure 3.2: Scheme of a quantum memory based on cavity EIT. a) Input pulse with a state that is a superposition of 0 and 1 photon impinges the cavity, which is coupled to the $|3\rangle \longleftrightarrow |1\rangle$ transition. The atom is initially in the state $|1\rangle$ and has a control field coupling the transition $|3\rangle \longleftrightarrow |2\rangle$. b) When the pulse enters the cavity, the control field is turned off so that the transparency window closes. c) With the control field off, the atom absorbs the field excitation, transferring its superposition to the atomic ground states. d) To recover the stored state, the control field is turned back on, the atom coherently emits the light, maintaining its initial superposition if none logical operation is performed in the atom during the storage period.

Finally

$$|\psi_{final}\rangle = \alpha|0\rangle_{field}|1\rangle_{\text{atom}} + \beta|0\rangle_{field}|2\rangle_{\text{atom}} = |0\rangle_{field}(\alpha|1\rangle_{\text{atom}} + \beta|2\rangle_{\text{atom}}).$$

That is, the initial state of light, a superposition of 0 and 1 photon, is transferred to an atomic state, a superposition of the ground states of the atom $|1\rangle$ e $|2\rangle$.

Once the state is stored in the atom, one can recover it after a storage time, simply by adiabatically turning the control field back on. The storage time is limited by decoherence effects [6], however, it should be clear that here we are not taking this into account. The storage time can be limited by the dephasing of the electronic states, γ_2 and γ_3, but here we consider them null in such a way that the efficiency is does not become lower for a longer storage time, i.e., the storage time does not play a role in the efficiency in our simulations, although including these effects is trivial.

The main advantage in using cavity EIT instead of EIT in free space is the significantly increase of the atom-field coupling provided by the cavity. With a higher coupling, the storage process occurs in a more coherent way, being less susceptible to dissipative effects and decoherence. Figure 3.2 shows how the storage process happens with cavity EIT.

3.2 Master equation description

The master equation formalism is the same introduced when the electromagnetically induced transparency was discussed. As it was shown before, the dynamics of a single three-level atom in the Λ configuration trapped in an optical cavity is governed by the master equation 2.13.

Here, however, we are going to work with all the detunings being null. So, finally, we have this simple form of the Hamiltonian

$$H_I = (\varepsilon a + \varepsilon^* a^\dagger) + (g a \sigma_{31} + g a^\dagger \sigma_{13}) + [\Omega_C \sigma_{32} + \Omega_C^* \sigma_{23}]. \tag{3.1}$$

Now, if we want to use this model to describe a quantum memory made up of this system, we have to make a few alterations in our Hamiltonian. First, the pump field is no longer an always turned on field, instead we are going to give it a Gaussian dependency in time

$$\varepsilon(t) = E_m e^{-\frac{1}{2}\frac{(t-t_0)^2}{\alpha^2}}. \tag{3.2}$$

This probe field is what we are interested in storing in the atom. To do so, we also must turn off the control field, making the atom absorb the probe, and we also have to turn the control field back on so we can restore the probe field stored in the atom. We do this by giving a time dependency to the control field of the form

$$\Omega_C(t) = \Omega_C^{MAX} \frac{1}{2} \{ [1 - tanh(\zeta_1(t - t_1))] + [1 + tanh(\zeta_2(t - t_2))] \}, \tag{3.3}$$

where ζ_1 controls the rate at which we turn off the control field and ζ_2 controls the rate at which we turn on the control field. This time dependency was not picked for any particular reason, it is just a way to smoothly turn off and on the control field.

Chapter 4

Results

In this chapter we show and discuss our results for a quantum memory based on cavity EIT. First, we simulate the experiment done by H. P. Specht et al. [6]. Once that is done, we begin our optimization of the efficiency. For this end, we select one parameter to vary and lock all other parameters. We begin with the maximum amplitude of the control field Ω_C^{MAX}. Next, we investigate ζ, that controls the velocity by which we turn off and on the control field. In the following, we study the dependency of the efficiency on t_1, the time chosen to turn off the control field. This is done by fixing a value for the time t_0 when the input pulse has its maximum, and varying t_1. Afterwards, the dependency of the efficiency on the atom-field coupling g is investigated. In this part are shown curves for the efficiency as a function of g, for selected values of the full width at half maximum (FWHM) of the input pulse, as well as different values of its amplitude ε, which has to be sufficiently small so that the probability of two or more photons inside the cavity is null. Lastly, the efficiency as a function of the number of atoms is investigated. After the optimization, a discussion on reflection and transmission losses is made, and seen as the main reason for the limitation of the efficiency in our current model. Next, using an approach developed by H. Carmichael [14], a quantum memory is simulated for a single photon input, and through a small modification we also simulate for a weak coherent pulse input. Due to the results obtained, we turn our attention to an input-output theory and revisit the relation between the field inside and outside the cavity. A small discussion on the role of phase-matching conditions on the memory efficiency is made, followed by a discussion on the right choice of the experimental setup. It's worth mentioning that all the figures in this document were obtained with simulations using the Quantum Toolbox in Python (QuTiP) [15].

4.1   Simulating the Experiment

Our first step, now that we have our model ready, is to try and reproduce the experiment of the single atom quantum memory [6] with ours simulations.
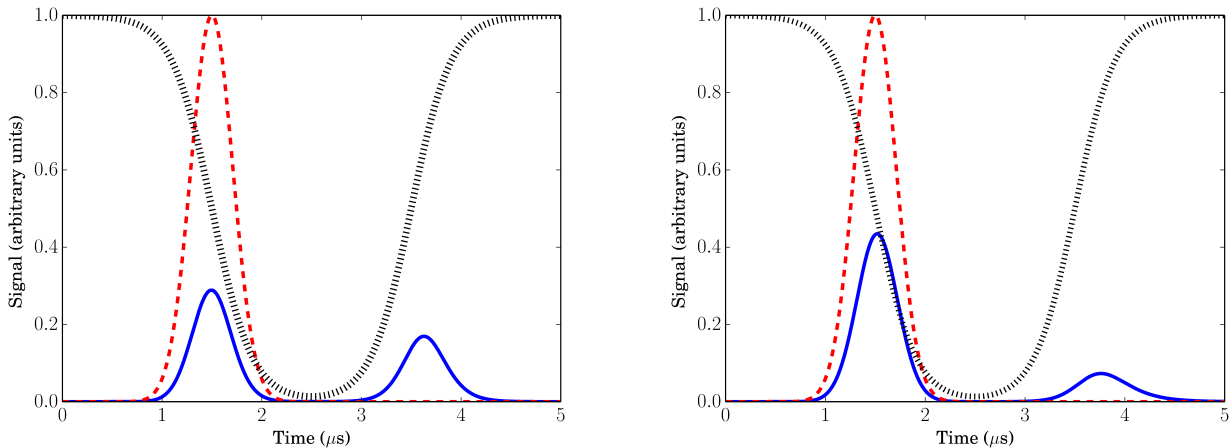
Figure 4.1: Single atom quantum memory scheme. The control field Ω_C, black dotted curve, is initially at its maximum value. Then we send in the input pulse ε, red dashed curve, at which point we slowly turn off the control field. The solid blue curve shows the mean number of photons in the cavity, and as the control field is turned off, the photons are absorbed by the atom. Later on, when we want to recover the pulse, we simply turn the control field back on. The parameters used here were: $\kappa/2\pi = 2.5$MHz, $g = 2.0\kappa$ in the left and $g = 1.09\kappa$ in the right, $\Omega_C^{MAX} = 2g/3$, $E_M = \sqrt{10^{-4}}\kappa$, $\zeta_1 = \zeta_2 = \zeta = 1.5$MHz, and $FWHM = 1.0\mu s$. We obtained an efficiency of 17.49%

In Figure 4.1 a) we try to use the same parameters mentioned in the reference [6]. The result is that we obtained an efficiency of 17.49%, which is almost twice as much as the 9.3% value of the experiment.

So, what's wrong with our model? The first thing we can point out is that we don't take into account oscillations of the atom in the cavity, i.e., we don't consider any deviations in the value of the coupling constant g. In real experiments the atom moves inside the cavity, leading to a time dependent atom-field coupling, which is sometimes close to its maximum value, but also occasionally close to its minimum one. Another effect of the motion of the atom in the cavity is that it experiences different stark shifts in the dipole trap. Due to this, an exact value of the atomic resonance is not possible to be known.

Figure 4.1 b) show us the result if consider an effective coupling $g = 1.09\kappa$. The efficiency is remarkably close to the value obtained in the experiment, 9.35%. As we said before, we considered an effective coupling constant to take into account the motion of the atom in the cavity. This was the same approach used in a previous experiment using the same system [16] to fit the experimental data to the theoretical curves.
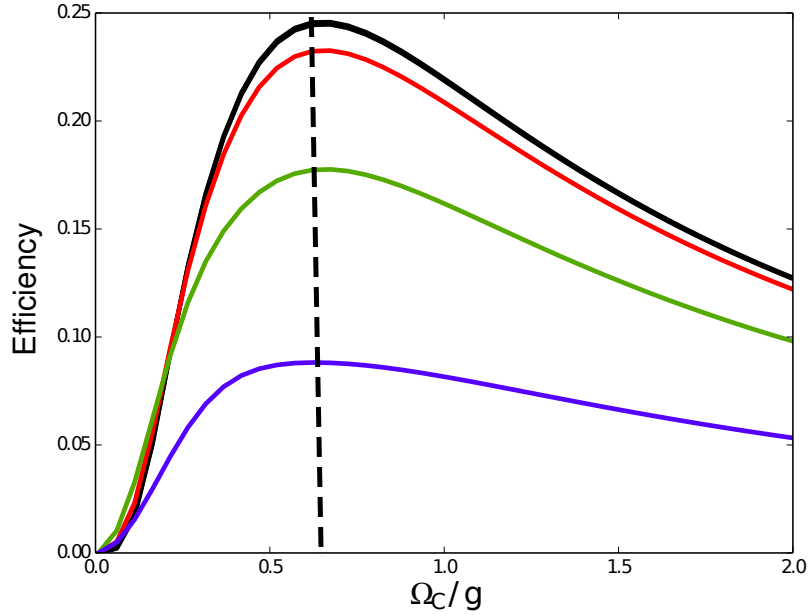
Figure 4.2: Efficiency in function of Ω_C^{MAX}. The parameters used here were: $\kappa/2\pi = 2.5MHz$, $\Gamma_{31} = \Gamma_{32} = 0.6\kappa$, $\zeta_1 = \zeta_2 = 1.9MHz$, $E_M = \sqrt{10^{-4}\kappa}$, $FWHM = 1.0\mu s$ and $g = 1\kappa$ in the blue curve, $g = 2\kappa$ in the green curve, $g = 5\kappa$ in the red curve and $g = 15\kappa$ in the black curve.

4.2 Optimizing the efficiency

4.2.1 Optimizing the efficiency as a function of Ω_C

Here we investigate what's the dependency of the efficiency on the maximum value of the control field Ω_C^{MAX}, for different values of g. It is important to stress that throughout the optimizations made, unless said otherwise, an input pulse with a fixed intensity and full width at half maximum was used.

In Figure 4.2 we see that for all values of g, we have a peak in the efficiency around $\Omega_C^{MAX} = 0.6g$ and $\Omega_C^{MAX} = 0.7g$. The behavior exhibited in this graph is due to the fact that the width of the frequency window in the EIT transmission spectrum for this system depends both on Ω_C and g. So, from now on, we are going to fix the value of Ω_C^{MAX} at $2g/3$.

4.2.2 Optimizing the efficiency as a function of ζ

Other parameters that could have an import role in the efficiency are ζ_1 and ζ_2, that determine how fast we turn off and on the control field.

First we are going to say that $\zeta_1 = \zeta_2 = \zeta$, and we investigate how the overall efficiency depends on this parameter. Figure 4.3 show us that we have a peak in the efficiency for $\zeta = 1.75MHz$.
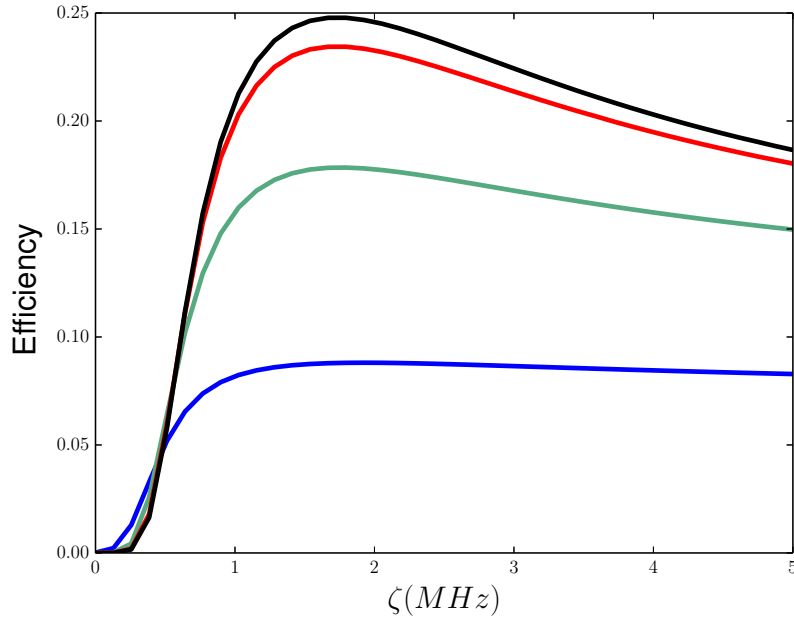
Figure 4.3: Efficiency as a function of $\zeta_1 = \zeta_2 = \zeta$. The parameters used here were: $\kappa/2\pi = 2.5MHz$, $\Gamma_{31} = \Gamma_{32} = 0.6\kappa$, $\Omega_C^{MAX} = 2g/3$, $E_M = \sqrt{10^{-4}}\kappa$, $FWHM = 1.0\mu s$ and $g = 1\kappa$ in the blue curve, $g = 2\kappa$ in the green curve, $g = 5\kappa$ in the red curve and $g = 15\kappa$ in the black curve.

Now we are going to look how ζ_1 and ζ_2 separately affect the efficiency. First we see the dependency of the efficiency on ζ_1.

Figure 4.4 a) show us a very similar dependency of the efficiency on ζ_1 to the dependency of the overall efficiency on ζ. Moreover the peak is in the same point, $\zeta_1 = 1.75MHz$.

In Figure 4.4 b) we plot the dependency of the efficiency on the parameter ζ_2. Unlike ζ_1, ζ_2 shows little effect on the efficiency for sufficiently large ζ_2, and for the greater the value of the coupling constant, smaller is the impact of ζ_2 on the efficiency.

From now on we fix the values of ζ_1 and ζ_2 at $1.75MHz$.

4.2.3   Optimizing the efficiency as a function of t_1

Another parameter that could influence the efficiency is the time we choose to turn off the control field relatively to the time the pulse enters the cavity.

Figure 4.5 show us indeed that when the difference between the center of the probe field pulse, t_0, and the time we choose to turn off the control field, t_1, is null, we have the best efficiency. One should also notice that if the parameter $\zeta = \zeta_1 = \zeta_2$ is changed, the best value for $t_1 - t_0$ also changes, but the maximum efficiency is lower.
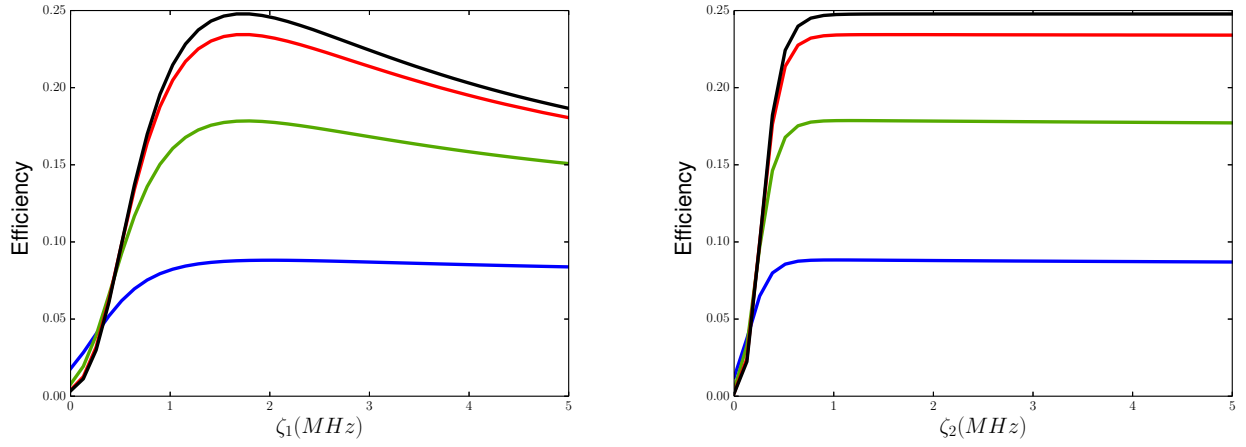
Figure 4.4: Efficiency in function of ζ_1 on the left and as a function of ζ_2 on the right. The parameters used here were: $\kappa/2\pi = 2.5MHz$, $\Gamma_{31} = \Gamma_{32} = 0.6\kappa$, $\Omega_C^{MAX} = 2g/3$, $E_M = \sqrt{10^{-4}\kappa}$, $FWHM = 1.0\mu s$ and $g = 1\kappa$ in the blue curve, $g = 2\kappa$ in the green curve, $g = 5\kappa$ in the red curve and $g = 15\kappa$ in the black curve.
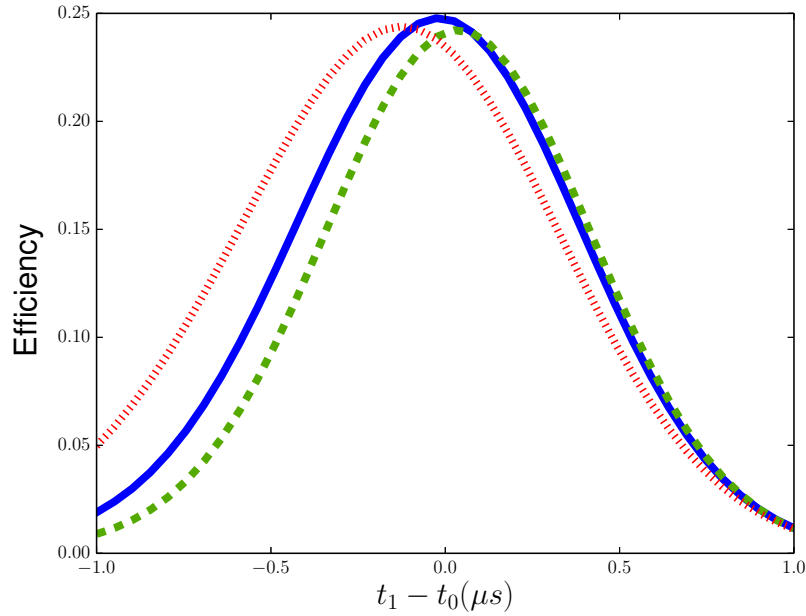

Figure 4.5: Efficiency as a function of $t_1 - t_0$. The parameters used here were: $\kappa/2\pi = 2.5MHz$, $\Gamma_{31} = \Gamma_{32} = 0.6\kappa$, $\Omega_C^{MAX} = 2g/3$, $E_M = \sqrt{10^{-4}\kappa}$, $FWHM = 1.0\mu s$, $\zeta = 1.25MHz$ (red dotted curve), $\zeta = 1.75MHz$ (blue solid curve), $\zeta = 2.25MHz$ (green dashed curve) and $g = 20\kappa$.
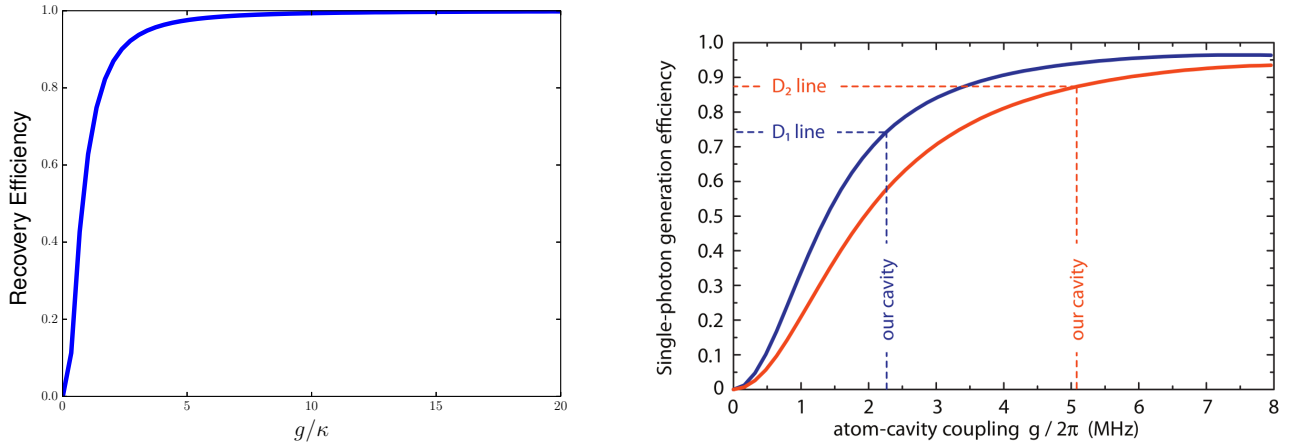
Figure 4.6: Recovery efficiency as a function of g (left) and single photon generation efficiency from the reference [17] (right). The parameters used on the left figure were: $\kappa/2\pi = 2.5MHz$, $\Gamma_{31} = \Gamma_{32} = 0.6\kappa$, $\Omega_C^{MAX} = 2g/3$, $E_M = \sqrt{10^{-4}\kappa}$, $FWHM = 1.0\mu s$ and $\zeta = 1.75MHz$.

4.2.4   Optimizing the efficiency as a function of g

Finally, we now investigate how the efficiency is affected by the coupling constant g.

First, lets look at how the coupling g affects the recovering efficiency. We define the recovering efficiency as the ratio between what the atom emits divided by what the atom absorbs.

Figure 4.6 a) show us that for sufficiently large g, the recovering efficiency tends to 100%. It is clear that for a sufficiently high coupling the recovery efficiency reaches 100%. A similar situation is shown in figure 4.6 b), taken from reference [17], where the single photon generation efficiency is studied. In the former case, the single photon generation efficiency also reaches values close to 100% for sufficiently high atom-field coupling. In both cases what is being studied is the ability of transferring the atom excitation to the field mode, and, as expected, both cases show similar results.

Now, lets look at the dependency of the efficiency, what the atom emits divided by what we sent to the cavity, on the coupling g.

Figure 4.7 show us that for this set of parameters, the efficiency saturates at about 25%, no matter how large g is.

However, as we said, this is the case for this set of parameters. What would happen if we changed things a little? Perhaps there is some parameter that is limiting the efficiency.

For different values of ε

Here we plot the same graph of efficiency against coupling g, but now for different values of the amplitude of the probe field. This amplitude must be small enough so that the probability of more than one photon in the cavity is null.
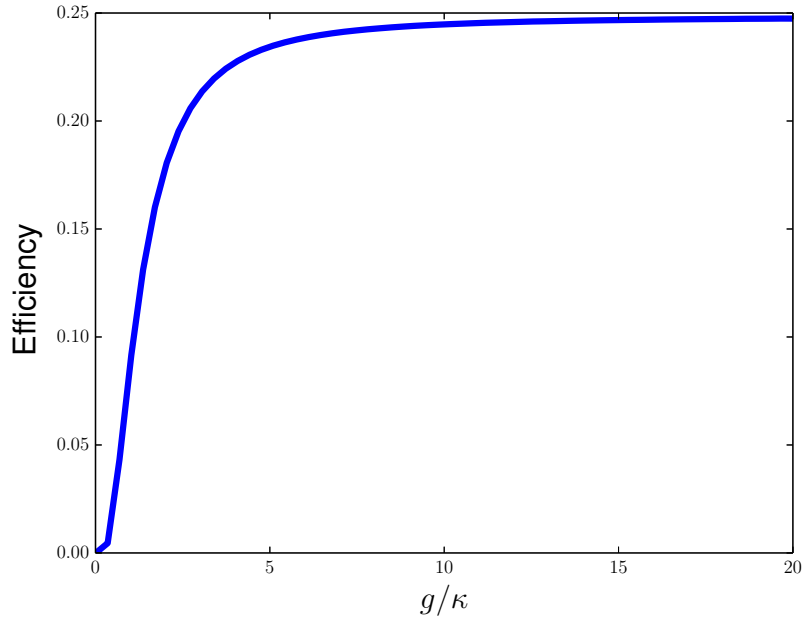
Figure 4.7: Efficiency as a function of g. The parameters used here were: $\kappa/2\pi = 2.5MHz$, $\Gamma_{31} = \Gamma_{32} = 0.6\kappa$, $\Omega_C^{MAX} = 2g/3$, $E_M = \sqrt{10^{-4}}\kappa$, $FWHM = 1.0\mu s$ and $\zeta = 1.75MHz$.

Figure 4.8 show us that if we raise the amplitude of the probe field the efficiency actually is decreased. Lowering further more the amplitude of the probe field makes no difference, as the efficiency saturates at the same value.

For Ω_C varying with g, $\Omega_C = 0.66g$, and Ω_C fixed

Before we continue, one thing important to point out is that the efficiency only saturates at 25% because we are letting Ω_C^{MAX} change with g. If we let Ω_C fixed in a particular value, making g larger would only decrease the efficiency, as we see in Figure 4.9.

The explanation to this is simple. By letting Ω_C^{MAX} vary with g, we are fixing the size of the dark-state window. By making Ω_C^{MAX} constant, as we raise the value of the coupling, the dark-state window gets smaller and smaller, to the point that our probe pulse is no longer inside that window of frequencies. So perhaps what's limiting our efficiency is that our probe pulse is not totally inside the window of frequencies provided by the dark-state.

For different values of FWHM

At this point we turn our investigation to how the full width at half maximum (FWHM) of the probe pulse affects the efficiency. Here the FWHM of the probe pulse is in the time domain, so a small value of FWHM in time, results in a pulse with a large number of frequencies. Conversely, a large value of FWHM in time gives a pulse with a small variation in frequencies.
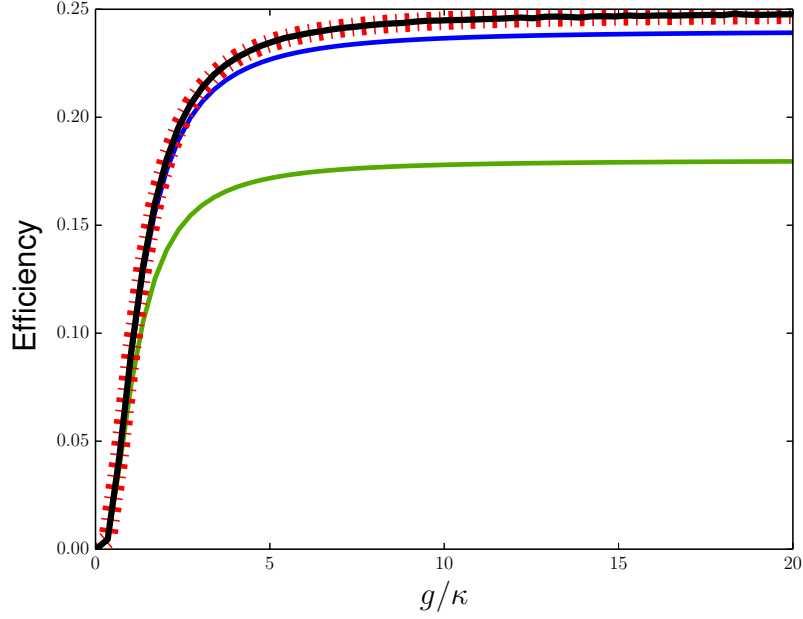
Figure 4.8: Efficiency as a function of g for different values of E_M. The parameters used here were: $\kappa/2\pi = 2.5 MHz$, $\Gamma_{31} = \Gamma_{32} = 0.6\kappa$, $\Omega_C^{MAX} = 2g/3$, $FWHM = 1.0\mu s$, $\zeta = 1.75 MHz$ and $E_M = \sqrt{10^{-1}}\kappa$ in the green curve, $E_M = \sqrt{10^{-3}}\kappa$ in the blue curve, $E_M = \sqrt{10^{-4}}\kappa$ in the black curve and $E_M = \sqrt{10^{-5}}\kappa$ in the dashed and dotted red curve.
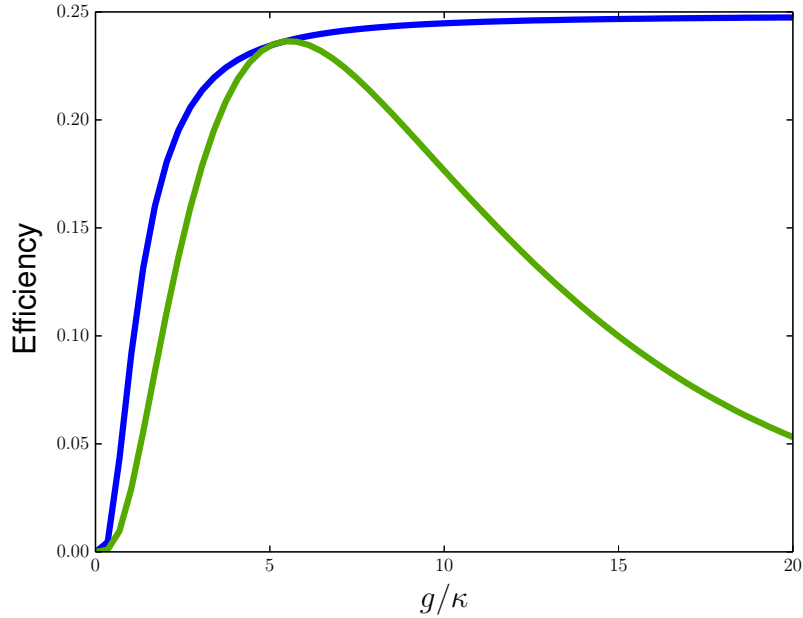

Figure 4.9: Efficiency in function of g for Ω_C^{MAX} varying with g, $\Omega_C^{MAX} = 0.66g$ in the blue curve and Ω_C fixed at $0.66 \times 5\kappa$ in the green curve. The other parameters used here were: $\kappa/2\pi = 2.5 MHz$, $\Gamma_{31} = \Gamma_{32} = 0.6\kappa$, $\zeta = 1.75 MHz$, $FWHM = 1.0\mu s$ and $E_M = \sqrt{10^{-4}}\kappa$.
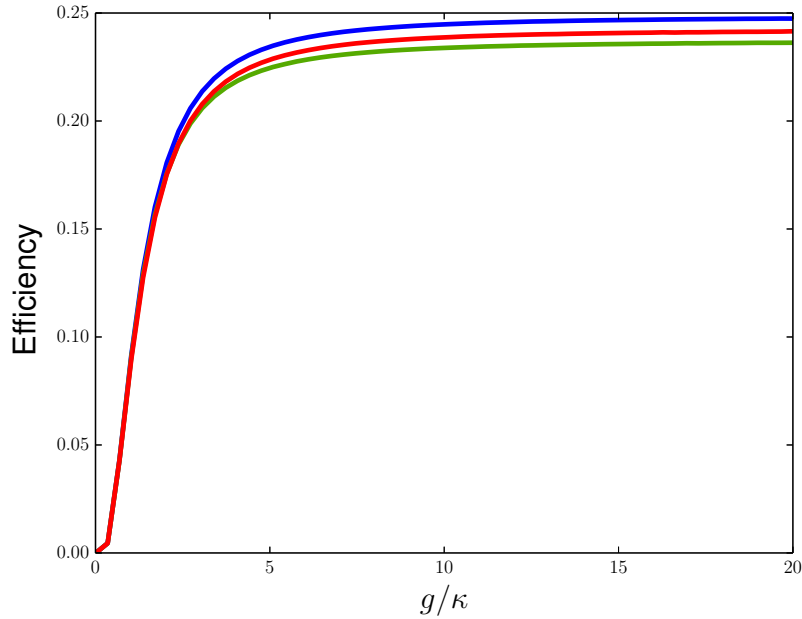
Figure 4.10: Efficiency as a function of g for different values of the FWHM. The parameters used here were: $\kappa/2\pi = 2.5MHz$, $\Omega_C^{MAX} = 2g/3$, $\Gamma_{31} = \Gamma_{32} = 0.6\kappa$, $\zeta = 1.75MHz$, $E_M = \sqrt{10^{-4}}\kappa$ and $FWHM = 1.3\mu s$ in the green curve, $FWHM = 1.0\mu s$ in the blue curve and $FWHM = 0.7\mu s$ in the red curve.

Figure 4.10 show us the dependency of the efficiency on g, for $FWHM = 0.7\mu s$, $FWHM = 1.0\mu s$ and $FWHM = 1.3\mu s$. Surprisingly, raising the value of FWHM, i.e., making the pulse fit better in the dark-state window, actually lowers the efficiency.

If we take the Fourier transform of our probe field pulse and plot it against the transmission spectrum of a cavity EIT process with the parameters we are using, the result is shown in Figure 4.11. We see that for $FWHM = 1.0\mu s$, the probe pulse is already inside the dark-state window. However this does not explain why making the pulse smaller in the frequency domain would lower the efficiency of the process.

Perhaps, what happens here is that increasing the $FWHM$ of the pulse, i.e., making it longer in time, prevents the system from absorbing it, since here we are maintaining Ω_C^{MAX} and ζ constant. If we recall the dynamics of this experiment, we slowly turn off the control field Ω_C as the pulse enters the cavity so the atom can absorb it. In this situation, without adjusting Ω_C^{MAX} and ζ properly, a longer pulse wouldn't completely enter the cavity in time to be absorbed by the atom, having a portion of itself still outside the cavity, and thus being reflected.
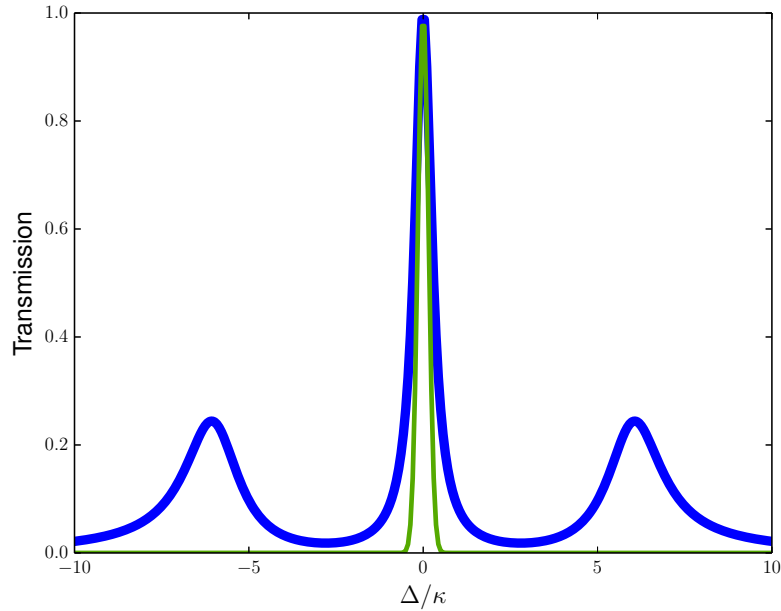
Figure 4.11: Cavity EIT transmission spectrum, i.e., the normalized mean number of photons inside the cavity versus the detuning Δ between the probe and cavity frequencies, blue curve, and our incident pulse's Fourier transform, green curve. It's clear that the pulse is within the dark-state range of allowed frequencies.

4.2.5 Optimizing the efficiency as a function of the number of atoms

One final parameter that can be investigated is the number of atoms. It may be that the efficiency is saturating at 25% because we don't have enough receivers to absorb the incoming pulse. So, here we see how the efficiency varies with the control field Ω_C^{MAX}, with ζ and with the coupling constant g for two, three and $N = 10000$ atoms.

Efficiency as a function of the control field

Here, as we can see in Figure 4.12 a), we studied de dependency of the efficiency as a function of the control field, for two atoms.

For two atoms, the best value of the amplitude of the control field is $\Omega_C^{MAX} = 0.8g$. Next, in Figure 4.12 b) the same graph, now for three atoms.

In a system with three atoms, the best value for the control field amplitude is $\Omega_C^{MAX} = 1.15g$.

Finally, we investigate the same scenario for $N = 10000$ atoms. For this end, a semi-classical model was solved, i.e., starting from the master equation 2.13, we derived equations of motion for the operators. A full quantum model would lead to a infinite set of linear differential equations. To overcome this, we make the approximation $\langle a\sigma \rangle = \langle a \rangle \langle \sigma \rangle$. With this, one goes from a infinite set of linear differential equations to a finite set of nonlinear differential equations [11]. The results achieved are shown in Figure 4.12 c).
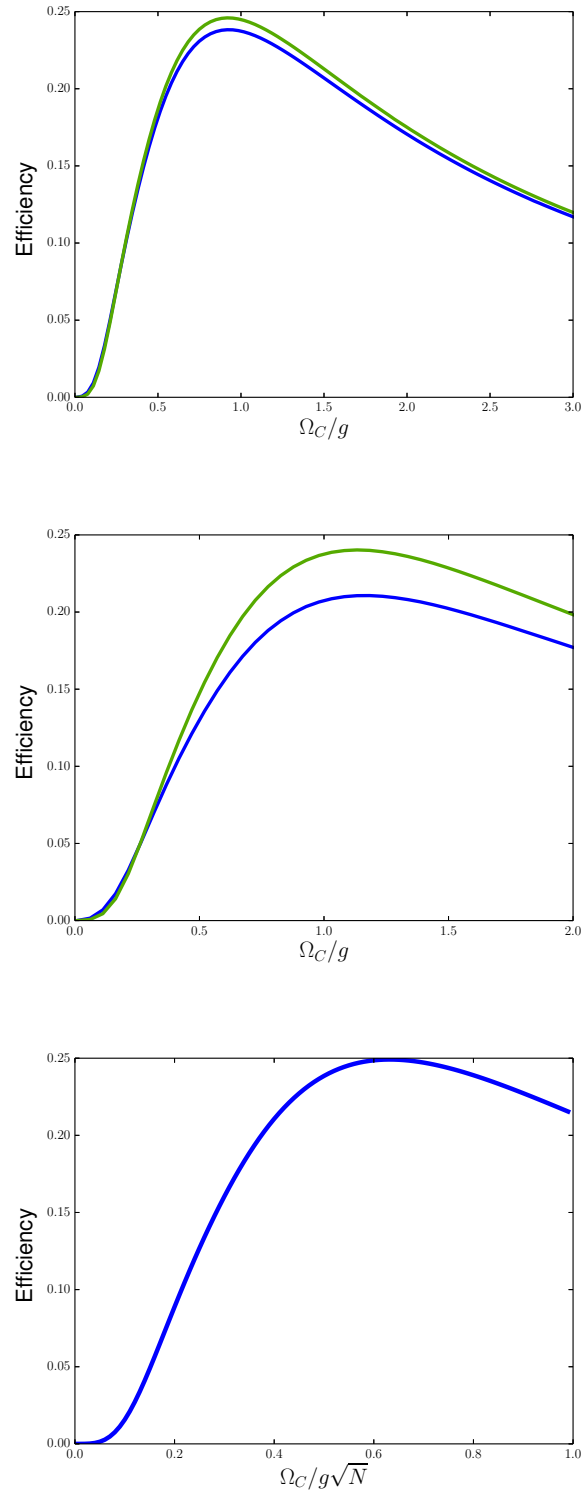
Figure 4.12: Efficiency of the system as a function of the control field for two atoms (up), three atoms (middle) and N atoms (down). The parameters used here were: $\kappa/2\pi = 2.5MHz$, $\Gamma_{31} = \Gamma_{32} = 0.6\kappa$, $\zeta = 1.75MHz$, $FWHM = 1.0\mu s$, $E_M = \sqrt{10^{-4}}\kappa$ and $g = 5\kappa$ in the blue curve and $g = 15\kappa$ in the green curve for the left and middle graphs and $g = 5\kappa$ for the right graph.
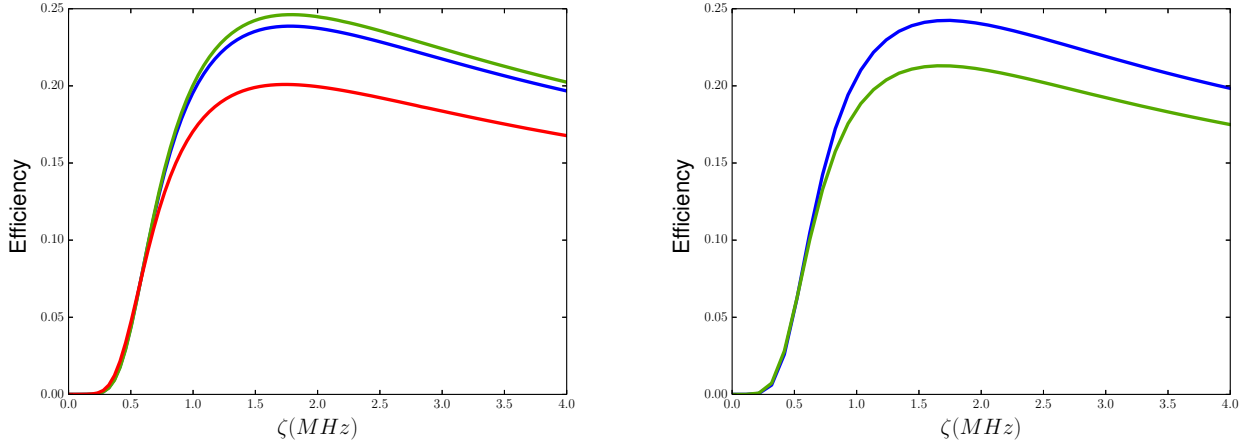
Figure 4.13: Efficiency as a function of $\zeta_1 = \zeta_2 = \zeta$ for two atoms. The parameters used here were: $\kappa/2\pi = 2.5MHz$, $\Gamma_{31} = \Gamma_{32} = 0.6\kappa$, $FWHM = 1.0\mu s$, $E_M = \sqrt{10^{-4}}\kappa$ and $g = 2\kappa$ in the red curve, $g = 5\kappa$ in the blue curve and $g = 15\kappa$ in the green curve.

Now, with $N = 10000$ atoms in the cavity, we see that the optimum value for the control field amplitude is $\Omega_C^{MAX} = 2g\sqrt{N}/3$.

Efficiency as a function of ζ

Here, we investigate how the efficiency varies with ζ for two and three atoms in the cavity.

In Figure 4.13 a) we can see that, as it was for one atom, the best value is $\zeta = 1.75MHz$. Figure 4.13 b) show us the same situation, optimum ζ at $1.75MHz$, showing that the number of atoms has none or little effect on the parameter ζ.

Efficiency as a function of the coupling constant

Once established the best value of the control field for each of the configurations of the system, with two, three or $N = 10000$ atoms, we investigate the efficiency of the system in function of the coupling constant, for each of the system's configurations.

Figure 4.14 a) show us the same behavior that we encountered for one atom. Moreover, the efficiency saturates at the same value, 25%.

In Figure 4.14 b), we see again the same behavior encountered for one and two atoms, and with the efficiency still saturating at 25%.

Finally, in Figure 4.14 c), we plot the efficiency in function of the coupling constant g for a cavity with $N = 10000$ atoms. Here the efficiency saturates much faster than before, but still at 25%.

From our results, it becomes clear that, as expected, increasing the number of atoms has the same effect as having only one "super atom" with cooperativity $\sqrt{N}C$, where C is the

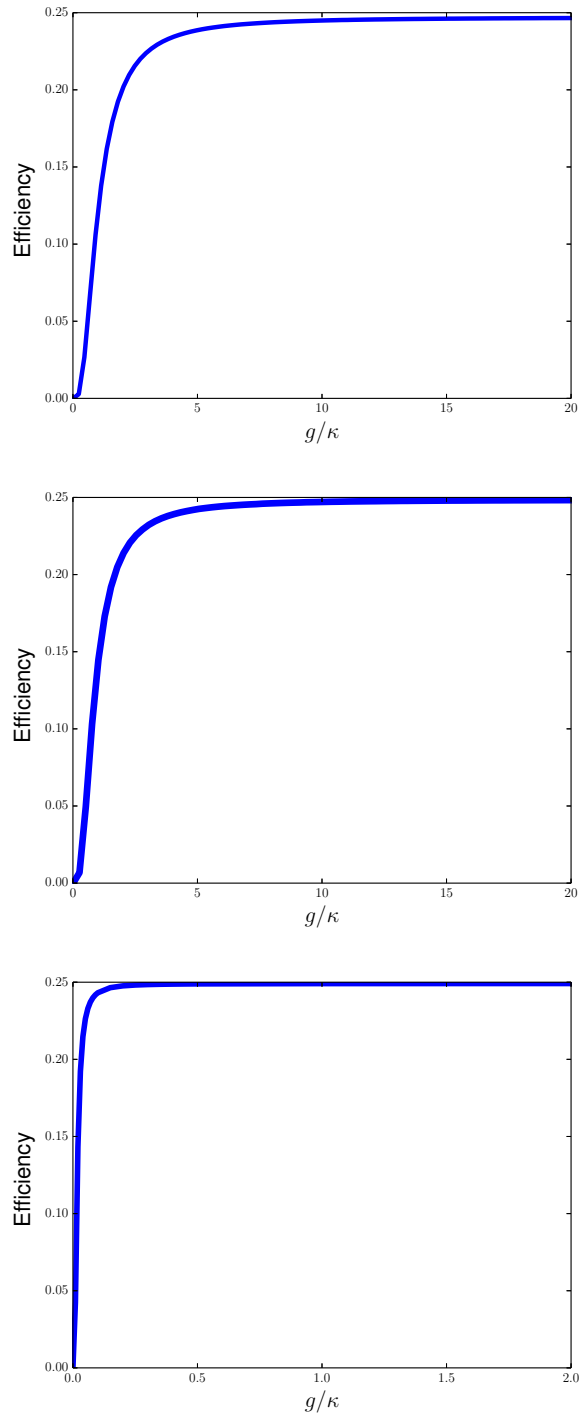Figure 4.14: Efficiency as a function of the coupling constant g for two atoms (up), three atoms (middle) and N atoms (down). The parameters used here were: $\kappa/2\pi = 2.5MHz$, $\Gamma_{31} = \Gamma_{32} = 0.6\kappa$, $FWHM = 1.0\mu s$, $E_M = \sqrt{10^{-4}}\kappa$ and $\Omega_C^{MAX} = g$ (left), $\Omega_C^{MAX} = 1.15g$ (middle) and $\Omega_C^{MAX} = 2g\sqrt{N}/3$ (right). It is clear that the efficiency saturates at 25%.
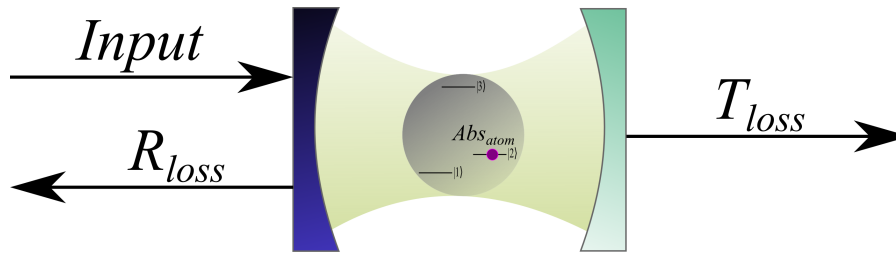
Figure 4.15: Reflection and transmission losses. Upon impinging the left mirror, which is highly reflective, part of the light is reflected from the cavity, disregarding the light that would be reflected even without the presence of the atom, we have our reflection losses R_{loss}. Part of the light that enters the cavity is absorbed by the atom and stored as a population of the level 2, which is the Abs_{atom} part. Finally, there's some portion of light that exits the cavity without interacting with the atom, our transmission losses, which is the T_{loss} in the figure.

cooperativity for a single atom.

4.3 Reflection and transmission losses

As it is shown in Figure 4.7 we can see that the efficiency saturates at 25%. But why is that? To understand why this happen we must look at the relation between the transparency window of the EIT, which is proportional to $\left|\Omega_C^{MAX}\right|^2/g^2$ [16], and the frequency width $\Delta\omega_p$ of the probe pulse. To put the pulse inside the cavity its $\Delta\omega_p$ must be smaller than the transparency window of the EIT, which requires a strong Ω_C^{MAX} and/or weak atom-field coupling g. But doing so, we have a strong transmission so that we lose energy/information by the transmission of the system. To avoid this high transmission we must decrease the Rabi frequency of the control field (and/or increase the atom-field coupling g). But in this case we will end up with a transparency window of the EIT narrower than $\Delta\omega_p$, implying a high reflectivity for the probe pulse (see inset of Figure 4.16). So, the explanation for the low memory efficiency is that the light is either reflected before entering the cavity or that it is transmitted before it could interact with the atom. This situation is illustrated in Figure 4.15.

To quantify the losses, for a experimental setup as illustrated in Figure 2.3, one knows that the cavity transmission is given by [18]

$$T_{loss} = 2\kappa\langle a^\dagger a\rangle, \tag{4.1}$$

which evaluated when the input pulse is interacting with the atom represents the portion of light that is not absorbed and is lost by transmission. The light absorbed by the atom is simply given by

$$Abs_{atom} = \langle\sigma_{22}\rangle. \tag{4.2}$$

Finally, from energy conservation, one can extrapolate that the portion of light that is reflected upon impinging the cavity is the light that would enter and then leave an empty cavity minus the transmission loss and the part absorbed by the atom, i.e.,

$$R_{loss} = \langle n \rangle_{emptycavity} - T_{loss} - Abs_{atom}. \tag{4.3}$$

Normalizing these quantities to the mean number of photons that enters an empty cavity, $\langle n \rangle_{emptycavity} = 2\kappa \langle a^\dagger a \rangle_{emptycavity}$, we have that

$$R_{loss} + T_{loss} + Abs_{atom} = 1. \tag{4.4}$$

Something important to remember is that there is another possible source of energy loss, which is incoherent emission from the excited level $|3\rangle$, given by $2(\Gamma_{31} + \Gamma_{32})\langle \sigma_{33} \rangle$. However, in all of our simulations the process are made in an adiabatic manner, in such a way that the excited level $|3\rangle$ is almost never populated and therefore losses due to its incoherent emission are negligible.

Figure 4.16 shows us the reflected part of the input coherent pulse, the part that is transmitted without interacting with the atom and the efficiency of the memory as function of the control pulse amplitude Ω_C^{MAX}.

In Figure 4.16 we see that at first we have a significant percentage of the incoming pulse being reflected, for small values of Ω_C^{MAX}. So, in order to let the pulse enter the cavity, we increase the control field amplitude Ω_C^{MAX}, so that the transparency window increases. However, by doing that we raise the percentage of light that is transmitted without interacting with the atom. This happens since with a large Ω_C^{MAX} the atom is transparent, so that now the incoming pulse passes right through, without interacting with the atom.

4.4   Single photon input

Here we explore how a single photon wave packet as the input state affects the memory's efficiency. To generate the single photon we use an auxiliary system, an approach described in [14]. This auxiliary system is composed of a three level single atom in the Λ configuration trapped inside a high finesse cavity, as our main system, and we use the protocol described in [19] to generate a single photon, as it is shown in Figure 4.17.

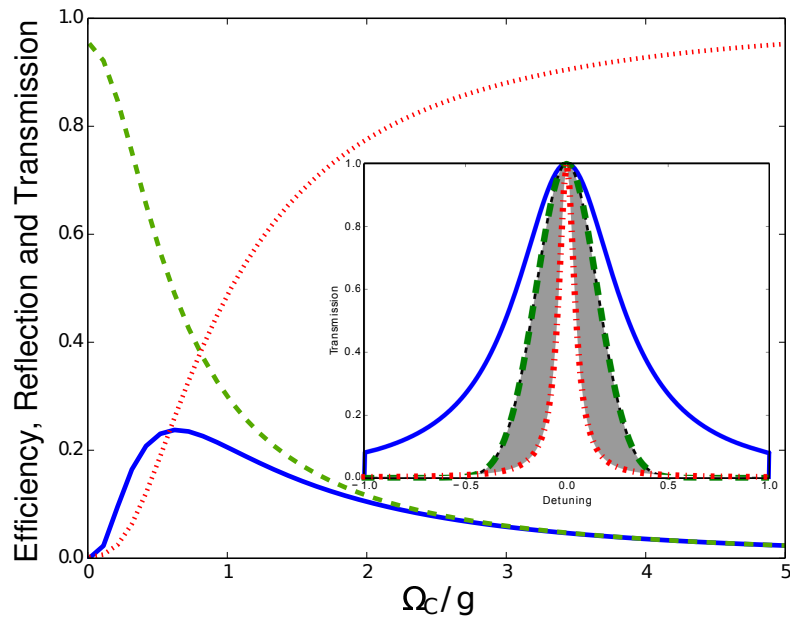The master equation for this system is given by

Figure 4.16: Transmission (red dotted curve) and reflection (dashed green) from cavity and efficiency of the memory (solid blue). The parameters used were: $\kappa/2\pi = 2.5 MHz$, $\Gamma_{31} = \Gamma_{32} = 0.6\kappa$, $g = 5\kappa$, $E_M = \sqrt{10^{-4}}\kappa$, $FWHM = 1.0\mu s$ and $\zeta = 1.75 MHz$. *Inset*: The blue solid curve is the EIT transparency window for a value of the control field Ω_{C_1}, the green dashed curve is our input pulse and the red dotted curve is the EIT transparency window for a value of the control field $\Omega_{C_2} < \Omega_{C_1}$. For the first value of the control field, Ω_{C_1}, the input pulse is completely inside the transparency window. However, this also means that the transmission of the system is very high and we can't turn off the control field fast enough so the atom can absorb it, so a big part of th input pulse is lost due to transmission. Conversely, for the second value of the control field, Ω_{C_2}, the input pulse is not completely inside the transparency window, and from the start a portion of the pulse (gray shadowed area) is immediately lost by reflection.
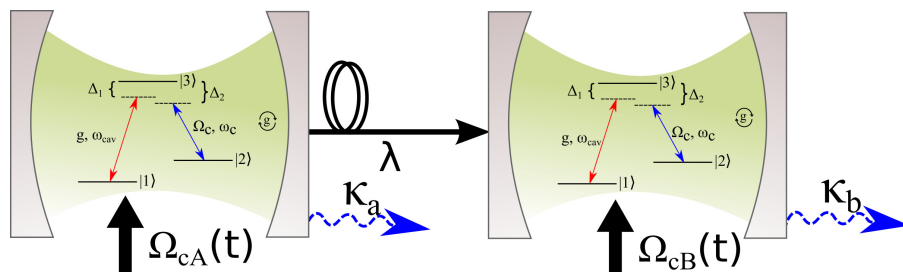

Figure 4.17: Scheme of the single photon input proposed by H. Carmichael [14]. In the first cavity a single photon pulse is generated, which is then sent to the second one, where the memory process occurs.

$$\frac{d\rho}{dt} = -i[H_i, \rho] + \kappa(2C\rho C^\dagger - C^\dagger C\rho - \rho C^\dagger C)$$
$$+ \sum_{\alpha=A,B} \Gamma_{31_\alpha}(2\sigma_{13_\alpha}\rho\sigma_{31_\alpha} - \sigma_{33_\alpha}\rho - \rho\sigma_{33_\alpha})$$
$$+ \sum_{\alpha=A,B} \Gamma_{32_\alpha}(2\sigma_{23_\alpha}\rho\sigma_{32_\alpha} - \sigma_{33_\alpha}\rho - \rho\sigma_{33_\alpha}) \tag{4.5}$$

where

$$C = \sqrt{\kappa_A}a + \sqrt{\kappa_B}b$$

and

$$H_i = g_A(a\sigma_{32_A} + a^\dagger\sigma_{23_A}) + g_B(b\sigma_{31_B} + b^\dagger\sigma_{13_B})$$
$$+ \Omega_{C_A}(\sigma_{31_A} + \sigma_{13_A}) + \Omega_{C_B}(\sigma_{32_B} + \sigma_{23_B})$$
$$+ i\sqrt{\kappa_A\kappa_B}(a^\dagger b - ab^\dagger). \tag{4.6}$$

The collapse operator C is defined in that way to take into account the indistinguishability of the source of photons impinging on the detector. This becomes more clear if one imagine a system composed of an arbitrary source of photons, a two level atom, and a detector, as is illustrated in Figure 4.18. If the atom is initially in the ground state, the photon emitted from the single photon source is first absorbed by the atom, which is promoted to the excited state, and goes back to the ground state emitting a photon which is then detected. If however the atom is initially in the excited state, the photon emitted by the single photon source can't be absorbed by the atom, so it goes directly to the detector. The detector can't distinguish the source of the photons, and the collapse operator C is defined in such a way to take that into account. This is the same situation as the one encountered with a single sided cavity system. Both the light reflected in the mirror and the one transmitted after entering the cavity go through the same path, making them indistinguishable to a detector. Therefore, the second cavity presented here in the H. Carmichael model is a single sided one. Nevertheless, the generalization to the second cavity being two sided should be straightforward.

In Figure 4.19 we can see how the efficiency changes with the coupling constant. It is clear that for a single photon wave packet input state, for a sufficiently large coupling constant, a near 100% efficiency is possible.

This is so because of the auxiliary cavity. In free space the portion of an incoming pulse that is not immediately absorbed by the system would get reflected. However, in our case, the incoming pulse is in another system, and is slowly transferred to our system of interest, making
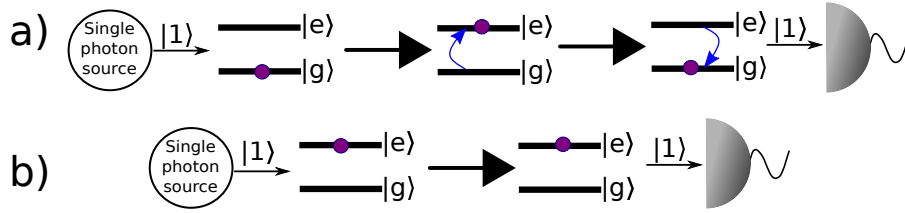
Figure 4.18: System composed of a single photon source, a two level atom and a detector. a) The atom is initially in the ground state $|g\rangle$. When a photon is emitted by the single photon source, the atom is promoted to the excited state $|e\rangle$ and it stays there for a certain amount of time. After this, the atom goes back to the ground state, emitting a photon in the process, which is then detected. b) Here the atom is initially in the excited state $|e\rangle$. When the single photon source emits a photon, it can't be absorbed by the atom, since it is already in the excited state, so the photon goes directly to the detector, where it is detected. In this two situations, the detector can't tell what is the origin of the photon: if is a photon emitted by the atom or if it was emitted by the single photon source. The detector can't distinguish photons from the atom and from the source, and that is the role the collapse operator C plays in the master equation, it accounts for the photons' indistinguishability in the detector.
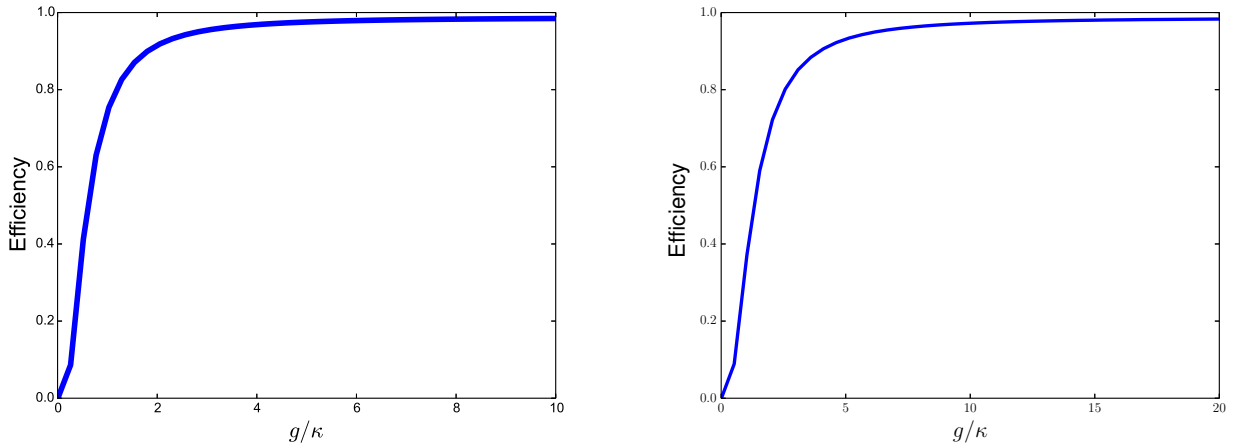
Figure 4.19: Efficiency as a function of the coupling constant g for the single photon input (left) and for the coherent pulse input (right). The parameters used on the left were: $\kappa_A/2\pi = 1.5MHz$, $\kappa_B/2\pi = 2.5MHz$, $\Gamma_{31A} = 10\kappa_A/9$, $\Gamma_{32A} = 8\kappa_A/9$, $\Gamma_{31B} = \Gamma_{32B} = 0.6\kappa_B$, $g_A = 15\kappa$, $\Omega_{CA}^{MAX} = 2g_A$, $\Omega_{CB}^{MAX} = 2g/3$, $\zeta = 2MHz$. The parameters used on the right were: $\kappa_A/2\pi = 2.5MHz$, $\kappa_B = \kappa_A$, $\Gamma_{31} = \Gamma_{32} = 0.6\kappa_A$, $\Omega_C^{MAX} = 2g/3$, $E_M = \sqrt{10^{-4}}\kappa_A$, $FWHM = 1.0\mu s$ and $\zeta = 1.75MHz$

it possible to be completely absorbed.

In order to bypass the efficiency limitation of the system, inspired by the work of H. Carmichael [14], we came up with a way to use the regime where the transmission is low (see Figure 4.16) and prevent the light from being reflected. To do this we added another cavity, identical to our original one, to our first model. In this scenario, the pulse first enters an empty cavity, that transmits this light to the second one which contains the atom. In this way, instead of coming at once to the cavity and inevitably being reflected, the pulse is slowly transmitted to the place of interest. The experimental setup is basically the same one illustrated in Figure 4.17 a), except that the first cavity is empty and a coherent input pulse is sent through it. It is important to stress that in our model we only consider the part of the pulse that enters the cavity. Experimentally, to put an entire single photon pulse inside a cavity, one has to use a time dependency for the pulse which is the time reverse of the cavity decay [20].

The master equation for this system is given by

$$
\begin{aligned}
\frac{d\rho}{dt} = &- i[H_i, \rho] + (2C\rho C^\dagger - C^\dagger C\rho - \rho C^\dagger C) \\
&+ \sum_{i=1,2} \Gamma_{3i}(2\sigma_{i3}\rho\sigma_{3i} - \sigma_{3i}\sigma_{i3}\rho - \rho\sigma_{3i}\sigma_{i3})
\end{aligned}
\tag{4.7}
$$

where

$$
C = \sqrt{\kappa_A}a + \sqrt{\kappa_B}b
$$

and

$$
H_i = \varepsilon(t)(a + a^\dagger) + g_B(b\sigma_{31_B} + b^\dagger\sigma_{13_B}) + \Omega_C(t)(\sigma_{32_B} + \sigma_{23_B}) + i\sqrt{\kappa_A\kappa_B}(a^\dagger b - ab^\dagger), \tag{4.8}
$$

and $\varepsilon(t)$ is given by Equation 3.2 and $\Omega_C(t)$ by Equation 3.3.

As it is shown in Figure 4.19 b), with this scheme we are able to obtain an efficiency greater than 98%.

4.5   Input-output theory with phase-matching condition

So far we've got two main results. First we've seen that for a coherent input pulse, the efficiency can't go any higher than 25%. On the other hand, using a scheme with two cavities, as proposed by H. Carmichael [14], both for a single photon and a coherent input pulse, an efficiency close to 100% was achieved, which shows that there should not be any considerable difference in the results if the input pulse is in a single photon Fock state or in a coherent state. However, in
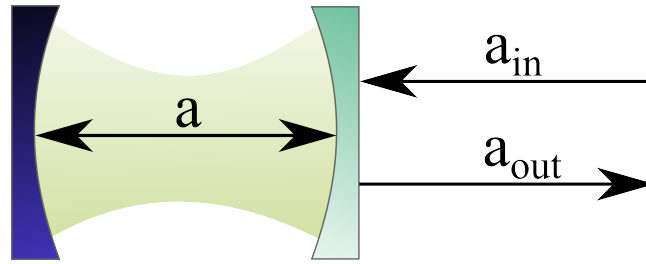
Figure 4.20: Scheme of a single sided cavity with its internal mode, a, the input mode a_{in} and the output mode a_{out}. The left mirror is perfectly reflective, while the right one is partially reflective, in such a way that the field can only enter and exit the cavity by one side.

the past years phase-matching conditions derived from an input-output theory were developed, ensuring, for a system with a single cavity, efficiencies near 100%. These phase-matching conditions generally rely on the destructive interference of the field immediately reflected as the input pulse impinges the cavity mirror (ϕ_r), and the field that enters the cavity and then is transmitted to the outside again after one round trip (ϕ_t). If ϕ_r and ϕ_t completely destroy each other, then the input pulse can only be inside the cavity, where it is absorbed by the atom. The ramification of imposing that ϕ_r and ϕ_t completely annihilate each other is an expression for the time dependency of the control field $\Omega_C(t)$ depending on the temporal shape of the input pulse $\phi(t)$, such that $\Omega_C(t) = \Omega_C(t, \phi(t))$. More recently, using this approach, J. Dilley et al. [21] showed that for a sufficiently high cooperativity $C = g^2/\kappa\gamma$, one can obtain an efficiency arbitrarily close to 100%. Nonetheless, this result disagrees with our first conclusion that the efficiency must be limited to 25% for a single cavity system. To solve this apparent conundrum we must investigate further how both models reach theirs results.

4.6 Revisiting the relation between the field inside and outside the cavity

The input-output theory gives a simple relation between the cavity mode and the external modes. For a single sided cavity, the input mode a_{in}, the cavity mode a, and the output mode a_{out}, are connected through a differential equation given by [8]

$$\dot{a}(t) = -i[a(t), H_s] - \kappa a(t) + \sqrt{2\kappa}a_{in}(t),$$

where κ is the cavity field decay rate, H_s is the system's Hamiltonian and a, a_{in} and a_{out} satisfy the relation [8]

$$a_{in}(t) + a_{out}(t) = \sqrt{2\kappa}a(t).$$

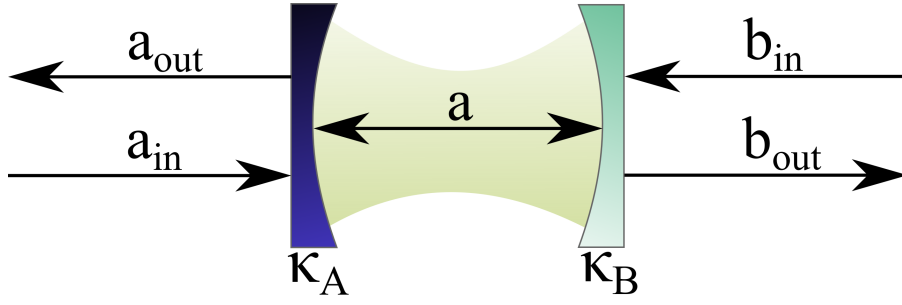The scheme described by these equations is illustrated in Figure 4.20.

Figure 4.21: Scheme of a two sided cavity. On the left we have the input mode a_{in} and the output mode a_{out} of the left mirror, which have a cavity field decay rate κ_A. Analogously, on the right side of the cavity we have the modes b_{in} and b_{out}, and a mirror with a cavity field decay rate κ_B. Finally, we have the internal mode a of the cavity.

The extension to a two sided cavity is straightforward, so that we have [8]

$$\dot{a}(t) = -i[a(t), H_s] - (\kappa_A + \kappa_B)a(t) + \sqrt{2\kappa_A}a_{in}(t) + \sqrt{2\kappa_B}b_{in}(t),\qquad(4.9)$$

with the relations

$$a_{in}(t) + a_{out}(t) = \sqrt{2\kappa_A}a(t),\qquad(4.10)$$

and

$$b_{in}(t) + b_{out}(t) = \sqrt{2\kappa_B}a(t).\qquad(4.11)$$

As it can be observed, here we have two input modes, a_{in} and b_{in}, two output modes, a_{out} and b_{out}, and two decay rates, κ_A and κ_B, for each side of the cavity, as it is shown in Figure 4.21.

This is the most general setup possible. Most often one would send an input through only one side of the cavity, say the left side for instance, so in this situation we can safely consider $b_{in} = 0$ for all times, which would leave us with

$$\dot{a}(t) = -i[a(t), H_s] - (\kappa_A + \kappa_B)a(t) + \sqrt{2\kappa_A}a_{in}(t),\qquad(4.12)$$

and

$$a_{out}(t) = \sqrt{2\kappa_A}a(t) - a_{in}(t),$$
$$b_{out}(t) = \sqrt{2\kappa_B}a(t).\qquad(4.13)$$

With this we have our first two important results: if one is sending an input through one side of a cavity and wishes to know what comes out of the other side, the output is related to the field inside the cavity through $b_{out}(t) = \sqrt{2\kappa_B}a(t)$. However, if the desired measurement is at the same side as the input is being sent, then the output field relates with the field inside the cavity through $a_{out}(t) = \sqrt{2\kappa_A}a(t) - a_{in}(t)$. What this expression tell us is that there's an interference process occurring between the field transmitted and the one reflected by the

mirror. It is important to remember that no assumptions were made other than that the input
occurs only through one side of the cavity.

Finally, for our system of interest, an atom inside the cavity, after some minor manipulation
Equation 4.12 yields

$$\dot{a}(t) = -ig\sigma_{13} - (\kappa_A + \kappa_B)a(t) + \sqrt{2\kappa_A}a_{in}(t). \tag{4.14}$$

With that in mind, lets return for a moment to the master equation approach. Although it is
a very powerful method to calculate the dynamics inside the cavity, it can be rather cumbersome
to derive relations for the fields inside and outside the cavity directly from this approach, as it
can be seen in [18]. That being said, it would be very useful to show an equivalence between the
two models, even if limited to certain conditions. From Equation 2.13, with the Hamiltonian
given by Equation 3.1, knowing that $\langle O \rangle = Tr(\rho O)$, $\langle \dot{O} \rangle = Tr(\dot{\rho} O)$, and $[a, a^\dagger] = 1$, it is easy
to show that

$$\langle \dot{a} \rangle = -ig\langle \sigma_{13} \rangle - \kappa\langle a \rangle - i\varepsilon. \tag{4.15}$$

Equations 4.14 and 4.15 are very similar, nevertheless, Equation 4.15 is in the limit where one
of the mirrors is perfectly reflective, so that there are no losses through that mirror. Performing
the same approximations in Equation 4.14 we have

$$\dot{a}(t) = -ig\sigma_{13} - \kappa_A a(t) + \sqrt{2\kappa_A}a_{in}(t). \tag{4.16}$$

Equations 4.16 and 4.15 are identical, with $-i\varepsilon = \sqrt{2\kappa_A}a_{in}$ and $\kappa = \kappa_A$. Since both
equations of motion for the field operator inside the cavity are equal, it implies that one can
use the relations 4.13 derived from the input-output theory to calculate the field outside the
cavity in the master equation approach.

So finally, we get to the root of the problem that limits the efficiency to 25%. The more
easily and straightforward attainable relation with the master equation approach for the field
inside the cavity and the output field is given by [18]

$$\langle a^\dagger_{out}a_{out} \rangle = 2\kappa\langle a^\dagger a \rangle. \tag{4.17}$$

Nonetheless, as we've seen previously and as it is stressed in [18], this relation is only valid
if the input field is null during the time interval in which the output field is being evaluated.
During this work it was always considered the usual experimental setup used to measure cavity
EIT, i.e., a two sided cavity. Since there is no interference process occurring between the
reflected and transmitted fields that forces a high intracavity field, reflection and transmission
losses are too substantial, so that in this setup the efficiency is limited to 25%. However,
it is easy to fix our model to consider a one sided cavity. For that purpose one only has
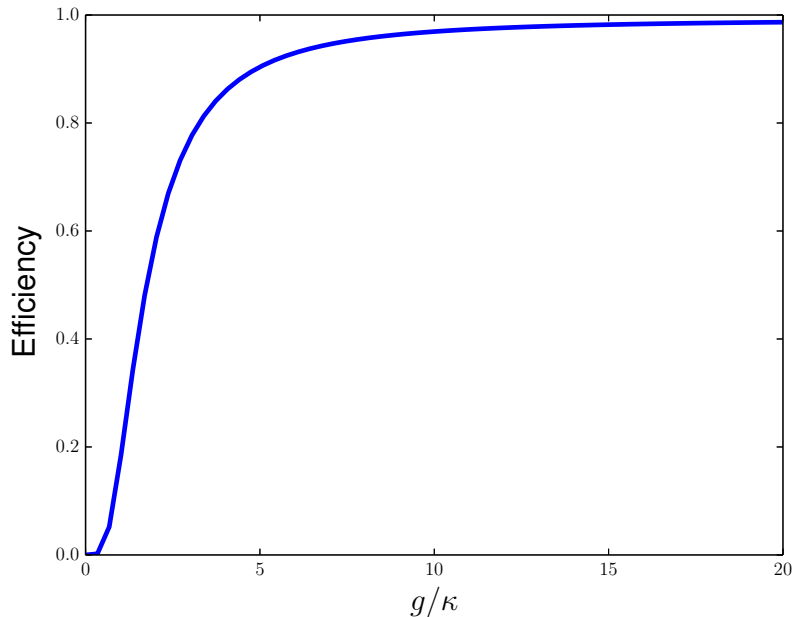
Figure 4.22: Efficiency as a function of the coupling rate g. Here the only modification to previous simulations with one cavity was the expression for the output field. The parameters used here were: $\kappa/2\pi = 2.5 MHz$, $\Gamma_{31} = \Gamma_{32} = 0.6\kappa$, $\Omega_C = 2g/3$, $E_M = \sqrt{10^{-4}\kappa}$, $FWHM = 1.0\mu s$ and $\zeta = 1.75 MHz$.

to use the relation $a_{out}(t) = \sqrt{2\kappa}a(t) - a_{in}(t)$ to calculate the field outside the cavity, since the master equation approach calculates the dynamics inside the cavity independently of the mirrors configuration, the only caution necessary is to know exactly which kind of setup one wishes to simulate so that after the master equation is solved, the output field can be obtained in the proper manner. This can be seen in Figure 4.22, in which the only modification to our model was the expression for the output field and now, as expected, for a sufficiently high value of the coupling constant g, efficiencies over 98% are acquired.

4.7 The role of the phase-matching condition in the memory efficiency

As it was shown in the previous sections, we were able to achieve an efficiency of over 98% for a quantum memory simply by choosing the best parameters for the system and adiabatically turning off and on the control field Ω_C. No phase-matching conditions were applied in our simulations, so one may wonder if they are of any use in real life applications. First of all, it is important to remember that the master equation theory used in this work is a very well established method for describing the dynamics of open quantum systems [7]. To include dissipation and different kinds of reservoirs is a trivial task, which is derived from first principles, in
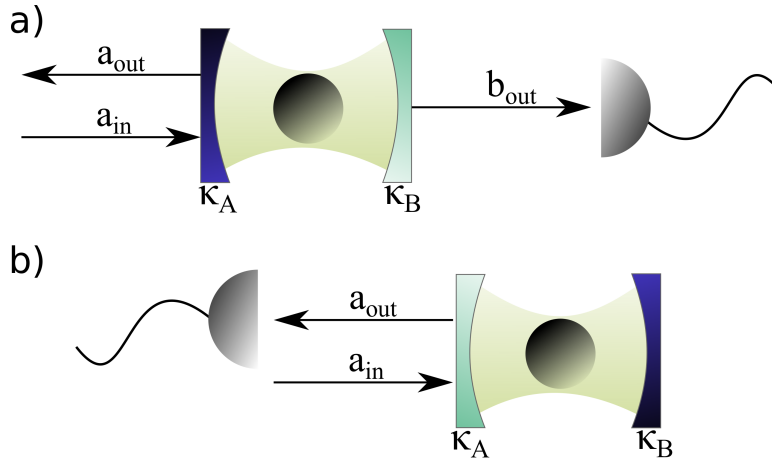
Figure 4.23: Cavity being probed through the higher reflective mirror (up) and through the lesser one (down). a) the input is made through the left mirror, which is highly reflective while the right one has a higher transmission rate in such a way that light leaves the cavity preferably through the right side, where a detector is placed. b) once again the input is made through the left mirror, which now has lower reflectivity than the right one in such a way that light leaves the cavity through the left side, where a detector is placed.

contrast with the input-output theory, in which dissipations are added *ad hoc* [8]. Nevertheless, despite the afore mentioned issues, the input-output theory does provide highly effective tools for treating cavity systems in a intuitive manner. For applications such as quantum repeaters, the results obtained in this work meet the requirements, but applications like linear optical quantum computing demand higher efficiencies, and that is where a more accurate control of the system efficiency, provided by phase-matching conditions for instance, might be needed.

4.8   Choosing the adequate setup

In Figure 4.23 we illustrate the two different experimental setups approached in this work. In setup a) we have a cavity where the left mirror is almost perfectly reflective and the right one has a considerable transmission. The input is made through the left side of the cavity and a detector is placed at the right side of it, so it can measure the transmitted light. In setup b) we have a cavity where the right mirror is almost completely reflective and the left one has a higher transmission. The input in this case is also made through the left side of the cavity, although, since the right mirror has a very low transmission rate in comparison with the left one, almost no light would pass through it and making transmission measurements through that side of the cavity extremely tardy, so a detector is placed at the left side of the cavity. It will detect both light that impinges the cavity and it is immediately reflected, and light that enters the cavity and them is transmitted back outside, as well as any interference that may arise from these sources.
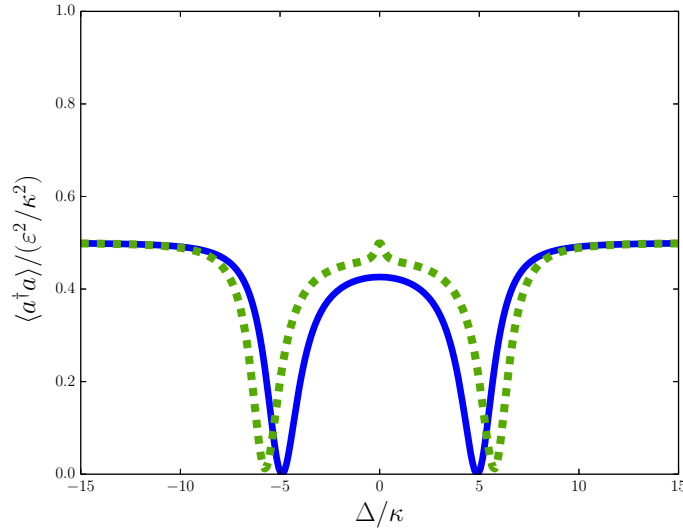
Figure 4.24: Normalized cavity transmission for cavity EIT with a single sided cavity (setup b)). In the blue solid curve the control field $\Omega_C = 0$, and in the green dashed curve the control field $\Omega_C \neq 0$. It is clear that these are not the desired curves and this experimental setup is not suitable for this kind of measurement.

It was already shown here that setup a), although the one used to measure cavity EIT, is unsuitable for a quantum memory experiment based on this phenomenon. Conversely, one can also show that setup b), albeit fit for a quantum memory experiment based on cavity EIT, it is absolutely inapt for the measurement of the phenomenon in which this quantum memory is based on.

In Figure 4.24 we have the theoretical curves for a cavity EIT experiment made with a single sided cavity (setup b) from Figure 4.23). In the solid blue curve, when the control field is off, the light is immediately reflected from the cavity when the detuning is null, for in this situation the probe is not in resonance with the system. The two minimums in the transmission are the resonances of the system. In the dashed green curve, when the control field is off, one can see a similar curve. Here, the light enters the cavity, but since now the system is transparent to the probe when the detuning is null, the light reflects back inside the cavity and is then transmitted outside to be detected. It is clear that these are not the desired curves, the phenomenon can't be observed properly, and another kind of experimental setup is needed.

It is also important to notice that the experiment [6] was realized in a limit where the transmission losses are almost negligible in comparison to the reflection ones, as it can be seen in Figure 4.16. So, although the model used in the result's first part of this work showed itself to be the wrong one for a quantum memory experiment, we still were capable of obtaining similar results to the ones obtained by H. Specht et al. [6].

Chapter 5

Conclusions

We have investigated the efficiency of a quantum memory based on EIT in optical cavities. When assuming an incoming weak coherent pulse and a single cavity we were able to show that there is a maximum efficiency of 25%, independently of the chosen values of parameters when there is no back reflection in the first mirror. In this case the efficiency is limited either by a high reflection or high transmission of the system. Adjusting the parameters to avoid a high reflection implies in a high transmission. On the other hand, adjusting the parameters to minimize the transmission implies in a high reflection. In both cases the atom can absorb a small part of the incoming pulse, limited to 25%. We were able to quantify the losses through reflection and transmission and established that for the efficiency to increase, the experimental setup must be changed.

We've also shown, following a model developed by H. Carmichael [14], that the nature of the input pulse, either being a single photon or a coherent state pulse, does not affect the efficiency obtained, which is nearly the same. This was necessary since in the past years works relying on input-output theory and phase-matching conditions, e.g., as it was done by Dilley et al. [21], with a single photon input pulse were developed, obtaining efficiencies arbitrarily close to 100% under certain conditions. With this the input pulse nature was discarded as a possible cause for the efficiency saturation at 25%, so that we were able to safely investigate other possible causes without disregarding an eventual major detail.

Since the phase-matching conditions were developed with an input-output theory, we decided to investigate it further and distinguish its main differences with the master equation approach. We successfully established an one to one correspondence between the two models, and identified their discrepancy that gives rise to such different results for the maximum efficiency. While the models developed using the input-output theory relied on a single sided cavity, our model was developed using the conventional setup used for cavity EIT experiments, i.e., a two sided cavity. This scheme, although ideal for observing the afore mentioned phenomenon, is far from suitable for a quantum memory experiment. In order to the input pulse to

be completely absorbed by the atom, an interference process between the reflected and trans-mitted portions of the input field must occur so that all light enters the cavity and remains there until is absorbed. A conventional cavity EIT setup doesn't allow this to happen, for reflected and transmitted light go through different paths. Nevertheless, we were able to show that the master equation approach does not have to be abandoned, since it perfectly calculates the dynamic inside the cavity, and the only modification needed appears when calculating the output field. We provided simple expressions for it, derived directly from the input-output theory, which, as mentioned before, proved equivalent to the master equation approach under the conditions we are working with.

Future developments might be in providing a more general correspondence between the two models under broader assumptions. Also, since the system here studied was a simple but reliable approximation of the real experimental situation, and it was shown that it can indeed achieve high efficiencies, it is interesting to investigate a more complete description of the system, e.g., to consider five or even eleven atomic levels instead of only three, as it is encountered in Rubidium atoms which are used in the experiments performed at MPQ [6, 16], investigate the possibility of efficiently store polarization states [6], implement quantum logic gates [22] and quantum error correction protocols [23], among other things.

References

[1] M. A. Nielsen and I. L. Chuang, *Quantum Computation and Quantum Information*, Cambridge University Press (2000).

[2] R. P. Feynman, Int. J. Theor. Phys. **21**, 467 (1982).

[3] A. I. Lvovsky, B. C. Sanders and W. Tittel, Nature Photonics **3**, 706 (2009).

[4] F. Bussières et al, Journal of Modern Optics, **60**, 1519-1537 (2013).

[5] C. Simon et al. Eur. Phys. J. D **58**, 1-22 (2010).

[6] H. P. Specht et al, Nature **473**, 190 (2011).

[7] H.P. Breuer and F. Petruccione, *The theory of open quantum systems*, Oxford University Press (2002).

[8] D. F. Walls and G. J. Milburn, *Quantum Optics*, Springer (2008).

[9] E. T. Jaynes and F. W. Cummings, Proc. IEEE **51**, 89 (1963).

[10] M. O. Scully and M. S. Zubairy, *Quantum Optics*, Cambridge University Press (1997).

[11] J. A. de Souza, *Controle das propriedades estatísticas do campo e biestabilidade óptica em eletrodinâmica quântica de cavidades (Control of the field's statistical proprieties and optical bistability in cavity quantum electrodynamics)*, PhD Thesis defended at the PPGF-UFSCar (2013).

[12] M. Fleischhauer, S.F. Yelin and M.D. Lukin, Opt. Comm. **179**, 395 (2000).

[13] D. J. Griffiths, *Introduction to Quantum Mechanics*, Pearson Prentice Hall (2005).

[14] H. J. Carmichael, Phys. Rev. Letters **70**, 2273 (1993).

[15] J. R. Johansson, P. D. Nation, and F. Nori, Comp. Phys. Comm. **183**, 1760 (2012). Comp. Phys. Comm. **184**, 1234 (2013). Further information and downloads at *http://qutip.org/*.

[16] M. Mücke et al., Nature **465**, 755 (2010).

[17] M. Mücke et al., Phys. Rev. A **87**, 063805 (2013).

[18] H. J. Carmichael, *An Open Systems Approach to Quantum Optics*, Springer-Verlag (1993).

[19] A. Kuhn, M. Hennrich, T. Bondo, G. Rempe, Appl. Phys. B **69**, 373 (1999).

[20] M. Bader et al., New Journal of Physics **15**, 123008 (2013).

[21] J. Dilley, P. Nisbet-Jones, B. W. Shore and A. Kuhn, Phys. Rev. A **85**, 023834 (2012).

[22] A. Reiserer et al., Nature **508**, 237 (2014).

[23] P. Barberis-Blostein et al., New Journal of Physics **12**, 023002 (2010).